UNIVERSITEIT•STELLENBOSCH•UNIVERSITY

jou kennisvennoot • your knowledge partner

Structural Design of a Stent for a Percutaneous Aortic Heart Valve

by

Anton Esterhuyse

Thesis presented at the University of Stellenbosch in partial fulfilment of the requirements for the degree of

Master of Mechanical Engineering

Department of Mechanical and Mechatronic Engineering
University of Stellenbosch
Private Bag X1, 7602 Matieland, South Africa

Supervisors:

Prof C. Scheffer Mr K. van der Westhuizen

March 2009

Declaration

I, the undersigned, hereby declare that the work contained in this thesis is my own original work and that I have not previously in its entirety or in part submitted it at any university for a degree.

Signature: .....
A.H. Esterhuyse

Date: .....

Abstract

Structural Design of a Stent for a Percutaneous Aortic Heart Valve

A.H. Esterhuyse

Department of Mechanical and Mechatronic Engineering
University of Stellenbosch
Private Bag X1, 7602 Matieland, South Africa

Thesis: MEng (Mech)

March 2009

Elderly patients suffering from aortic valvular dysfunction are often denied aortic valve replacement due to the fact that they are classified as too old and fragile to handle the physical stress of open-heart surgery and cardio-pulmonary bypass. There exists a need for an alternative solution which places less physical stress on the body. The development of a percutaneous aortic heart valve (PAHV), which may be implanted through a minimally invasive procedure, will provide a solution to old and fragile patients who otherwise have a very limited life expectancy. The development of such a device entails a costly and time-consuming process which involves a number of phases, including a prototype development phase, an *in-vitro* testing phase, an animal trial phase and a human trial phase.

This thesis focuses on the design and analysis of the stent component for a PAHV, suitable for implantation in sheep (animal trial phase). The process of developing a first prototype, involved an analysis of the stent

design requirements. This analysis was followed by a concept generation phase as well as comprehensive finite element (FE) analyses of the most promising concepts. The objective of the FE analyses was to determine the effects of a variation in strut width on the performance characteristics of the concepts. Based on the results of the FE analyses, final geometries were selected for each of the two most promising concepts. Subsequent to the selection of the final geometries, a number of prototypes were manufactured. The prototypes were subjected to an electro-polishing process. An experimental analysis was also conducted on the prototypes to evaluate the accuracy of the (FE) simulations as well as the actual performance of the stent prototypes.

The results of the FE analyses and experimental analyses indicated that strut width had a substantial influence on the parameters that were defined to characterise stent performance. The results of the analyses also highlighted the advantages and disadvantages of each concept and aided in identifying the concept that would be most suitable for the required application.

Limitations of the study were identified and recommendations were made to assist the continued research and development of the device.

Uittreksel

Strukturele Ontwerp van ’n Stent vir ’n Perkutane Aortiese Hartklep

(“Structural Design of a Stent for a Percutaneous Aortic Heart Valve”)

A.H. Esterhuyse

Departement Meganiese & Megatroniese Ingenieurswese
Universiteit van Stellenbosch
Privaatsak X1, 7602 Matieland, Suid Afrika

Tesis: MIng (Meg)

Maart 2009

Bejaarde persone wat aan aortaklepdisfunksie ly, word dikwels aortaklepvervanging geweier omdat hulle as te oud en swak geklassifiseer word om die fisiese stres van opehartchirurgie en kardiopulmonêre omleiding te hanteer. Daar is behoefte aan ’n alternatiewe oplossing wat minder fisiese stres op die liggaam plaas. Die ontwikkeling van ’n perkutane aortahartklep (PAHK) wat met ’n prosedure wat minimale ingryping behels, aangebring kan word, bied ’n oplossing aan persone wat oud en swak is en andersins ’n uiters beperkte lewensverwagting het. Die ontwikkeling van so ’n toestel is ’n duur en tydrowende proses wat heelwat fases behels, insluitende ’n prototipe-ontwikkelingsfase, ’n *in vitro*-toetsingsfase, ’n diertoetsingsfase en ’n menstoetsingsfase.

Hierdie tesis fokus op die ontwerp en ontleding van die stentkomponent vir ’n PAHK wat geskik is vir inplanting in skape (diertoetsfase). Die proses om ’n eerste prototipe te ontwikkel het eerstens ’n

ontleding van die stentontwerpvereistes behels. Hierdie ontleding is gevolg deur ’n konsepontwikkelingsfase sowel as omvattende eindige-elementontledings (EE-ontledings) van die mees belowende konsepte. Die doel van die EE-ontledings was om die gevolge van ’n variasie in stutwydte op die werksverrigtingeienskappe van die konsepte vas te stel. Na aanleiding van die resultate van die EE-ontledings, is finale geometrieë gekies vir elk van die twee mees belowende konsepte. Na die keuse van die finale geometrieë, is ’n aantal prototipes vervaardig. Die prototipes is onderwerp aan ’n elektropoleringsproses. ’n Eksperimentele ontleding is uitgevoer op die prototipes om die akkuraatheid van die EE-simulasies asook die werklike werkverrigting van die stentprototipes te evalueer.

Die resultate van die EE-ontledings en die eksperimentele ontleding het getoon dat stutwydte ’n wesenlike invloed op die parameters wat vasgestel is om stentwerkverrigting te karakteriseer, gehad het. Die resultate van die ontledings het ook die voordele en nadele van elke konsep uitgelig en ’n bydrae gelewer om die konsep te identifiseer wat die geskikste sou wees vir die vereiste toepassing.

Beperkings van die studie is geïdentifiseer en aanbevelings is gemaak om die verdere navorsing en ontwikkeling van die toestel te steun.

Acknowledgements

I would like to express my sincere gratitude to the following people and organisations who have contributed to making this work possible:

- My study advisors, Prof. Cornie Scheffer and Mr. Kobus van der Westhuizen for their patience, advice and valuable input during the project.
- A special thanks to Dr. Helmuth Weich and Prof. Anton Doubell from Tygerberg Hospital for organising the funding for the project as well as providing enthusiastic support during the project.
- Mr. Karl van Aswegen and Mr. Adriaan Smuts for making valuable contributions to the project. It was a tremendous pleasure working with you.
- Mr. Markus Lehmann from Disa Vascular for providing valuable advice and know-how as well as taking the time to set up and manufacture the stent prototypes.
- Mr. Cobus Zietsman and the staff of the department's mechanical workshop for manufacturing the taper expanders.
- Thank you to my friends and family for their endless support during the project.

Contents

List of Figures

List of Tables

Nomenclature

Variables:

D_{distal}^{load}	Instantaneous diameter at the distal end of the stent
$D_{central}^{load}$	Instantaneous diameter at the center of the stent
$D_{proximal}^{load}$	Instantaneous diameter at the proximal end of the stent
L^{load}	Longitudinal length before load removal
L^{unload}	Longitudinal length after load removal
D^{load}	Outer diameter before load removal
D^{unload}	Outer diameter after load removal
L^{crimp}	The crimped longitudinal length of the stent
L^{final}	The final deployed longitudinal length of the stent
σ_{max}	Maximum value of the element's predicted principle stresses
σ_{min}	Minimum value of the element's predicted principle stresses
S_e	Endurance limit
S_{ut}	Ultimate true tensile strength
$\frac{1}{FSF}$	Inverse fatigue safety factor

Abbreviations:

CAD	Computer Aided Design
FEM	Finite Element Method

FEA	Finite Element Analysis
FE	Finite Element
ISO	International Organisation for Standardisation
FSF	Fatigue Safety Factor
dia	Diameter

Glossary of Medical Terms:

Antegrade	Moving along the direction of the blood flow
Aortic arch	The superior left bend of the aorta between the ascending and descending portions
Aortic valve	A tri-leaflet valve situated between the left ventricle and the aorta
Catheter	A small tube inserted into a body cavity to remove fluid, create an opening, distend a passageway or administer a drug
Coronary	Refers to the circulation of blood in the blood vessels that supply blood to and from the heart muscle itself
Diastolic	Refers to the period of time during which the heart relaxes
Femoral artery	The vessel in the inguinal (groin) region that is often entered during a heart catheterization procedure
Guide wire	Device made of flexible metal used to guide placement of catheters in vascular surgery
Ischemia	A decrease in the blood supply to a bodily organ, tissue, or part caused by constriction or obstruction of the blood vessels
Mitral Valve	A bi-leaflet valve situated between the left atrium and the left ventricle
Neointimal	Refers to the scar tissue made up of cells and cell secretions that often forms as a result of vessel injury

	following angioplasty or stent placement as part of the natural healing process
Percutaneous	Refers to a procedure that is done through the skin
Regurgitation	Blood flow in the opposite direction from normal, as the backward flowing of blood into the heart or between heart chambers
Retrograde	Moving against the direction of the blood flow
Septum	The muscle wall that divides the heart chambers
Systolic	Refers to the period of time during which the heart contracts
Transseptal	Refers to a procedure performed through or across the septum

Chapter 1

Introduction

1.1 Background

The human heart contains four one-way valves that regulate the blood flow to and from the four chambers of the heart. Each of the valves consists of two or three cusps (leaflets) which prevent the back flow of blood when they are in the closed position. The aortic valve is the outlet valve of the main pumping chamber of the heart, the left ventricle. It is located between the left ventricle and the aorta, the primary blood vessel responsible for transferring blood to the rest of the cardiovascular system. During ventricular systole, the aortic valve opens to permit blood flow from the ventricle to the aorta. During ventricular diastole, back pressure causes the aortic valve to close, preventing the back flow of blood from the aorta to the ventricle.

Valvular heart disease occur when one or more of the heart valves are no longer capable of efficiently regulating the blood flow. The inlet (mitral) and outlet (aortic) valves of the left ventricle are the two valves that are most susceptible to disease and are responsible for the majority of clinical heart valve diseases [6]. It is estimated that valvular disease affects approximately 5% of the total human population [7].

There are two distinct valvular diseases that result in the malfunctioning of the aortic heart valve. Aortic valvular stenosis is an artificial

narrowing which restricts blood flow and causes an obstruction to the outflow of blood from the left ventricle. Aortic valve insufficiency is a weakening of the valve leaflets that results in regurgitation (back flow of the blood from the aorta to the ventricle) [6]. The most common causes for aortic stenosis are degenerative calcification of the valve leaflets, a disease related to aging, and a congenital bicuspid aortic valve [6].

There are various ways to treat Aortic Valvular Disease, depending on the type and severity of the disease. In some cases, medication alone is successful in treating the disease. In other cases, valvular repair may also be an option. If a patient is suffering from symptomatic severe degenerative aortic stenosis, a complete aortic valve replacement is required to ensure the long term survival of the patient [8]. Various types of aortic valve replacement prostheses are available, and the prosthesis selection depends on the type and severity of the disease. These valve prostheses include a range of mechanical valves, artificial tissue valves and animal tissue valves. The first aortic heart valve was implanted in 1952 [9]. Over the past 50 years, this technology has been researched and developed to the extent that, in the modern day, the implantation of these valves are common practice and a very high success rate is achieved.

1.2 Motivation

Despite the fact that it is performed with great success, an aortic valve replacement procedure is a massive operation which requires cardiopulmonary bypass (CBP) and places a major physical stress on the body. On top of this, the procedure is very expensive to perform, about R250 000 [10]. Elderly patients suffering from aoritc valvular dysfunction are often denied aortic valve replacement due to the fact that they are classified as too old and fragile to handle the physical stress of the procedure. As a result of this, in South Africa alone, each year around 2700 patients suffering from aortic valvular disease are classified as old or fragile and are subsequently denied valve replacement [10]. These patients have no choice but to wait for inevitable heart failure. As a result of the fact that

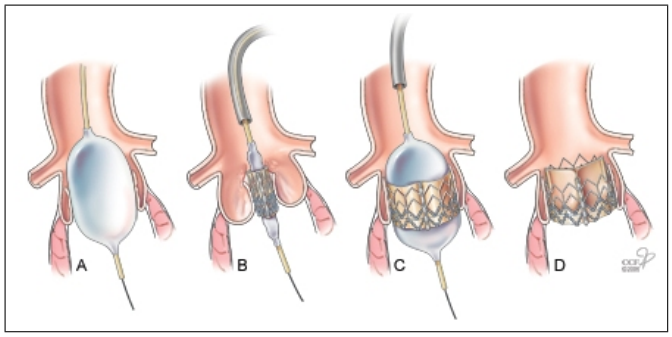

Figure 1.1: Percutaneous Aortic Valve Deployment [1]

there is no solution available to these patients, over the past ten years, research in the field of aortic valve replacements has shifted its focus to the development of aortic valves that may be placed with minimal invasive procedures. This has subsequently led to the development of the percutaneous aortic heart valve.

A percutaneous aortic heart valve comprises of three tissue leaflets mounted to an expandable stent frame. The expandable stent frame may either be a balloon expandable stent or self expandable shape-memory alloy stent. Both an antegrade and retrograde method have been developed to place the prostheses. For the retrograde approach, the prosthesis is first crimped onto a catheter. A guide wire followed by the catheter is then inserted into the femoral artery. The catheter is guided along the femoral artery, into the aorta, across the aortic arch and into the desired valve position (Figure 1.1 : B). Once in position the stent is expanded (balloon or self-expanding) and the valve open up like an umbrella to take the place of the diseased valve (Figure 1.1 : D). For the antegrade approach, the prosthesis is inserted, also via a catheter, through the rib cage and apex of the heart. This method is more invasive, however, it allows for larger prostheses to be deployed.

These prostheses are still in the medical trial phases and there are not yet any products available commercially. There are many reported difficulties associated with this type of valve [11; 12; 13]. These issues include difficulty in sealing the valves to prevent regurgitation; achieving a low profile, i.e. achieving a small device that is easy to navigate to

the desired position; deterioration of the leaflets and a limited life span; coronary obstruction and difficulty in achieving exact positioning of the valve. Additionally, there are very little published literature available regarding the development of these valves. This may be attributed to the fact that the development companies are very resolute to protect their intellectual property.

1.3 Research Objective

The Biomedical Engineering Research Group in collaboration with the Cardiology Department of the University of Stellenbosch have initiated a project to develop a percutaneous aortic heart valve that addresses the difficulties listed in Section 1.2. The project was sub-divided into three MScEng projects, each project focusing on a different aspect of the research project. The projects focused respectively on the valve leaflet design [5] and an analysis of the hemodynamic valve characteristics [4].

The present work relates to the structural development and analysis of the stent component for the valve prosthesis. Since many of the difficulties associated with these valves are directly related to the performance of the stent component, and since its performance plays a major role in the successful and efficient functioning of the prosthesis, the main objective of the study is to successfully develop and test a prototype stent component that addresses and solves these difficulties. Since a vital step in the product development cycle is the successful completion of the animal trial phase, the work will focus on developing a prototype that will be suitable for implantation in sheep (animal trial phase). Upon successful completion of the animal trial phase, the developed prototype may be scaled to human dimensions. The outcome of this thesis will provide a better understanding of the aspects that determine successful development of a stent for implementation in a percutaneous aortic heart valve.

1.4 Research Methodology

In order to achieve the objective as stated in Section 1.3 a thorough understanding of the field of stenting technology, the field of minimally invasive cardiac intervention and related fields is required. For this reason, a thorough literature review was conducted of the abovementioned fields, the results of which are presented in this thesis report. From the literature review as well as brain-storming sessions held with the development team, a list of engineering requirements for the stent component were identified. From these requirements a number of concepts for the stent component were developed.

The stent component of a percutaneous aortic valve prosthesis is an intricate device, involving complex geometries as well as several deformation modes. Due to the time and high cost involved in stent prototype manufacturing and testing, there existed a need for a low-cost approach to generate the required stress and deformation data to support the design of the device. This would aid in a better understanding of the mechanical characteristics of the device as well as minimise the number of design iterations required.

It was therefore decided to implement the finite element method (FEM) to analyse the forces and deformation modes that characterise the performance of the stent. The finite element (FE) package, MSC.Marc was selected to perform the analyses as it was capable of solving non-linear problems, it was compatible with the pre-processor package MSC.Patran, and both of these packages were availible at the University of Stellenbosch.

The generated concepts were first subjected to simplified finite element analyses (FEA) to identify the most promising concepts. From this, the two most promising concepts were identified and a complete structural finite element analysis was conducted for the stents in order to determine the structural characteristics of the stent models. The structural characteristics include aspects such as deployment pressure, dog-boning and coning, elastic recoil, plastic deformation and strain, and minimal

allowable crimping diameter. Elastic recoil refers to the elastic spring-back of the stent after the deployment pressure has been removed. The term "recoil" is preferred over "spring-back" as it is the generally accepted term used for stent design applications. Detailed definitions of these aspects are given in the text. From the results of the finite element analyses a strut width was selected for each stent component and ten prototypes were manufactured for each of the concepts. Tests were conducted on the prototypes to analyse the prototype performance as well as in an attempt to validate the numerical results of the finite element analyses.

From the results of the FEA as well as the experimental analyses, the advantages and disadvantages of each concept were identified and the concept most suitable for the application was identified. Limitations to the research conducted were identified and recommendations were made towards future work.

Chapter 2

Literature Review

2.1 Introduction

Successful development of a stent for the application in the percutaneous replacement of an aortic valve requires a thorough understanding of the design parameters and environment variables that determine the performance of the stent. It is also important to be acquainted with the scope and results of past research in the field as well as related fields and to identify the methods implemented to conduct the research. This enables the researcher to establish a new perspective into the field, to determine the shortcomings of the current research and to determine the context of the proposed research project. For these reasons, a thorough literature review was conducted into the field of percutaneous aortic valve replacement and related fields. The knowledge gained from the literature review is presented here.

The literature review discusses the results of recent animal and human trials, parameters that influence stent performance, current methodologies applied in the research, the challenges faced in current research as well as limitations of the current research. The context for the proposed research project is also established and finally, conclusions are drawn from the knowledge gained in the literature review.

2.2 Previous Medical Trials

2.2.1 Animal Trials

The first report of a successful percutaneous implantation of an aortic valve into an animal test subject was published in 1992 [12; 14]. In this study, stented valves were deployed successfully in seven pigs, however three of the pigs experienced complications associated with restriction of the coronary blood flow. The results of this study highlighted the importance of correct positioning of the prosthesis as well as taking coronary perfusion into account.

A number of animal studies have since been conducted [11; 12; 15]. These studies again brought to light the importance of designing the prosthesis to allow for coronary perfusion, employing a feasible positioning and alignment strategy and ensuring minimal prosthesis migration.

The results of a study conducted by Boudjemline and Bonhoeffer [16] on a group of lambs indicated that the percutaneous implantation of prosthetic aortic valves that are hemodynamically unnecessary and in which the native valves do not experience a minimal amount of back flow, will become covered in neointimal tissue, eventually rendering them incompetent. It is therefore a requirement that, for each animal used in a trial phase following prototype development, an aortic insufficiency must be established prior to the deployment of the valve. This may be done by means of aortic angioplasty [16] or a similar technique.

2.2.2 Human Trials

The first human implantation of a stented aortic valve was reported in December 2002 [17]. A short stent (14 mm) was used to minimize the risk of coronary obstruction while allowing deployment of the valved stent in the native position. The deployed stented valve functioned normally and no coronary obstruction occurred. The success of this procedure proved that with the use of a short stent and with the proper positioning of the

prosthesis it is possible to avoid coronary obstruction and interference with the mitral valve.

By 2005, Bonhoeffer had already implanted 81 valves in 75 patients with a 98% success rate [18]. CoreValve, a company who is currently developing a self expanding valve, has recently received approval for a European clinical trial involving 20 patients [19].

2.3 Desired Stent Attributes

According to a paper published by Poncin and Proft [20], the performance characteristics of a stent are directly related to the mechanical and physical properties of the material used to produce the stent. These performance characteristics include biocompatibility, X-ray and MRI visibility, radial strength, elastic recoil, flexibility, deliverability, profile, and long term integrity.

For an aortic valve stent a high radial strength is required to withstand the external compressive forces, imposed by the native aortic tissue, as well as the valve leaflet forces. recoil must be limited to a minimum to ensure the efficient anchoring of the device. Foreshortening must be restricted to a minimum en ensure the minimal deformation of the valve leaflets. The stent must exhibit a low profile to ensure the easy deliverability of the device and resistance to fatigue is important due to the cyclic forces imposed by the valve leaflets.

It is also known that a stent's geometric features have a major influence on the performance of a stent. It is therefore of interest to research the characteristics of the materials that are commonly used in stent applications and to analyze the performance impact of the various geometric properties of a stent.

2.3.1 Ideal material properties

The ideal properties of the material used to produce a stent are corrosion resistance, vascular compatibility, fatigue resistance and visibility

using standard X-ray and MRI equipment [20]. For balloon-expandable stents, a high elastic modulus will minimize recoil. A low yield strength is preferred to ensure that the balloon pressure required to produce the desired stent expansion is low enough (below five bar) to allow for manual pressurisation. A low yield strength is also required to enable effective stent crimping. High tensile properties will enable the volume of implanted material to be minimized while still achieving the required radial strength. This also allows the use of thinner struts to achieve an overall lower profile, improving flexibility and deliverability. A steep work-hardening rate provides the required rise in strength during expansion. A high ductility is advantageous as it is required to endure the deformation during expansion.

Some of the properties mentioned in the previous paragraph are related to each other in a conflicting manner. For this reason it is vital to determine the most significant material properties and accordingly achieve a cautious compromise between the materials available, in which some properties may be sacrificed for others.

2.3.2 Ideal tubing properties

Given that metal tubing is the most commonly used profile to produce stents, it is important to investigate how the tubing attributes influence the stent performance and manufacturability.

Typically, two distinct methods exist to produce tubing. These methods include welded-redrawn or seamless form. Despite modern welding techniques and advanced inspection systems, it is not possible to fully eliminate defects from the weld without localized micro-contamination and segregation [20]. Therefore it is preferable to utilize seamless tubing for stent applications.

The material properties of some materials are very sensitive to the tube drawing process. For this reason, a fine degree of control is required during the process to ensure repeatable properties for the tubing. The sensitivity however, provides the possibility to tailor the material

properties according to the requirements of the prosthesis. Tailoring of the material properties is only possible if the manufacturer has a sound knowledge of the detailed material behavior and tightly controls the process.

Materials with uniform and equally-axed small grain microstructures are generally preferred for polishing as well as resistance to fatigue and corrosion [21]. Minimizing the grain size will typically raise the yield strength with unfavorable consequences on recoil at crimping and expansion [20]. This is an example of properties that are related in a conflicting manner and, consequently, a compromise must be reached that will be best suited for the specific application.

Dimensional accuracy is also critical to stent performance and manufacturability [20]. A consistent wall thickness is required to achieve an even deployment of the stent. The majority of commercially availible stents are manufactured using a laser cutting process. It is of utmost importance to achieve a consistent strut width during the laser cutting process, which can only be achieved if the tubing has a consistent wall thickness. The outside diameter determines the accuracy of the guidance of the tube under the laser beam. For this reason, fine tolerances and tight cylindricity on the tubing is required.

The surface finish of the tubing is also an important factor to consider and must be smooth enough such that the cleaning and electropolishing procedures can achieve the desired stent finish.

Dimensional accuracy and surface finish are greatly influenced by the type of tube drawing process used. The floating and fixed plug drawing process produces the best geometry and surface finish [20]. However, this process is only possible if it is compatible with the selected material, required dimensions and the desired temper. An alternative process is the ductile core drawing technique. However, this process does not usually provide the same degree of accuracy achieved with hard tool techniques [20].

Although a fully annealed condition is preferred for the final stent, cold worked tubing is often used during the laser cutting process, fol-

lowed later by an annealing process. The subsequent annealing process should be adequately controlled to achieve the desired mechanical properties and microstructure. This approach minimizes the possibility of handling damage and relieves residual stresses imposed by the laser cutting process.

2.3.3 Influence of the geometric properties of a stent

It is known that stent design plays an important role in the restenosis rate of arteries and also the radial strength of the stent [22]. The strut thickness has also been linked to the endothelialization of the stent surface after implantation.

The sharp edges of the stent should be rounded to reduce the stress concentrations at the joints and to prevent the stent from cutting into the artery walls [22].

2.4 Modeling of Stent Behavior using FEM

A number of papers have been published on the finite element models constructed to perform non-linear simulations of stent behavior during crimping, expansion and stent-artery contact interaction. These simulations aim to accurately predict the time-dependant stresses and strains present during these processes. Application of finite element studies in this respect allows impact of various stent parameters to be analyzed without physically producing the stent or performing physical experiments. The impact of geometric design parameters on important stent performance characteristics such as radial recoil, foreshortening, stress concentrations and deployment pressure could be analyzed. The geometric design parameters include strut geometry, strut thickness and material selection to name but a few.

2.4.1 Strategies employed in finite element simulations

Due to the complexities involved in the processes that take place during the percutaneous implantation of a stented aortic valve, accurate simulation of these processes is a challenging task. For this reason, innovative methods must be implemented to simulate these processes in a simplistic manner, while maintaining the reliability of the results. The strategies employed to achieve this is described in this section.

2.4.1.1 Strategies employed to generate stent models

Published literature indicates that solid brick elements (C3D8), wedge elements (C3D6) and tetrahedral elements (C3D4) are commonly implemented in stent models [22].

For the finite element simulations, it is vital to ensure that the mesh of the model is sensitive enough, to ensure that the solution will converge to the correct answer [22]. However, a very fine mesh will result in an increase in the analysis time. For this reason, all possible measures should be taken to ensure that the solution converges, while limiting the analysis time to a minimum.

The balloons used to deploy the stents are often modeled as expandable cylindrical tubes [2]. The material type of the tubes is selected as polyurethane with equal material toughness and a bi-linear hyper-elastic (Mooney-Rivlin) model is implemented to represent the stress-strain behavior. The specific material properties for these materials are available in the literature [2].

2.4.1.2 Strategies employed to simulate the stent loading conditions

Due to the axial symmetry that is present in most stent geometries, it is often possible to use only the repeated symmetrical segment to simulate the deformation processes [2]. In these cases, it is very important to implement the correct boundary conditions on the nodes of the stent which are located in the plane of symmetry.

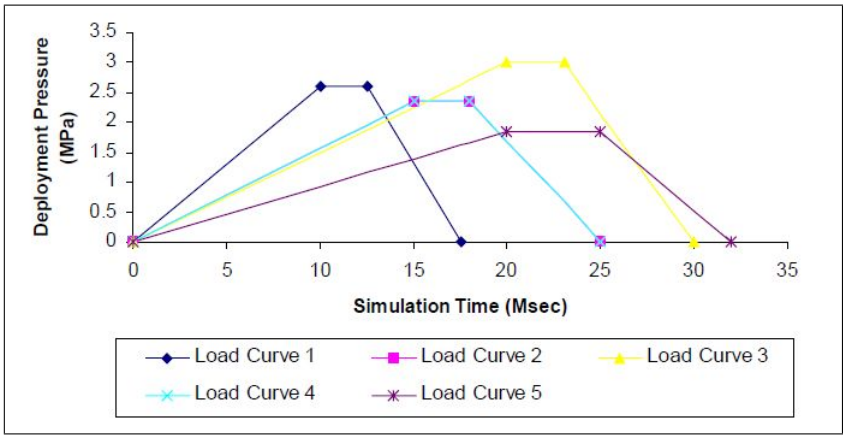

Figure 2.1: Pressure Load Functions [2]

The pressure loads are often simulated as a uniform surface load on the inner surface of the balloons (which are represented with cylindrical tubes) [2]. A three stage continuous linear function is used to represent this surface load. A ramp-up function is used to achieve the inflation of the balloon. A constant function is used to represent the expanded state of the balloon and a ramp-down function is used to achieve the deflation of the balloon. In such a case, the time duration of each stage is not very important, as a quasi-static solution is desired. It is however important to allow enough time for each stage to ensure that the solution converge to the equilibrium status. This approach ensures that the dynamic effects are limited to a minimum. Figure 2.1 shows a diagram of typical load functions used to simulate the pressure load.

When different stent geometries are compared to each other, it is required that the different geometries are compared in an impartial manner. To achieve this, the stents are expanded to a certain limit, for example a certain percentage of its failure strength, and the resulting stresses are analyzed and compared to each other.

2.4.1.3 Strategies employed in static deformation simulations

Experimental studies indicate that stent design have a significant impact on the long term clinical outcomes of patients undergoing coronary stent

placement [23; 24]. For this reason, it can be assumed that stent design will also have a major impact on the performance of percutaneous aortic heart valves. Since the crimping and expansion processes of the stent involve large deformations, the non-linearities of the stent materials must be carefully considered.

Results from static deformation simulations

Results of static deformation simulations found in the literature indicate that an increase in the number of struts in the circumferential direction of a stent results in more material available for expansion and subsequently produces a beneficial effect on the expansion in the radial direction [2]. However, an increase in the number of slots in the circumferential direction of the stent results in an increase in the elastic recoil.

The results also indicated that an increase in the strut width results in an improvement in the resistance against excessive elastic recoil as well as an increase in the resistance against compressive forces applied by the vascular wall after deployment. However, an increase in strut width will also increases the difficulty with which a stent expands during the inflation process and limits the flexibility of the stent. It is important to establish a balance between radial strength and flexibility of the stent.

A decrease in the crimp radius of a coronary stent results in an increase in the equivalent plastic strain [22]. This is of particular interest in the current project as a valve stent could possibly undergo large crimping deformations. The maximum Von Mises stress in the stent after expansion increases with an increase in the accumulated plastic strain [22]. Again, this is of particular interest in the current project as the valved stent may experience large accumulated plastic strain. If the maximum stress levels approach the ultimate stress for the material, this may become a problem.

The radial strength of the stent increases with accumulated plastic strain [22]. This means that the stent is stronger and that it is able to withstand more pressure from the arterial walls. Accordingly a stent which is

fabricated at a greater diameter and then crimped to its minimum diameter will have an increased radial strength.

Effect of deployed diameter

The radial force required to expand a stent increases as the deployment diameter increases [22], which means that there will be an increase in the stress levels. However, the radial recoil decreases with an increase in deployment diameter.

2.5 Fatigue-life Simulations

The stent implemented in a stented heart valve will be subjected to cyclic blood pressures as the heart beats, as well as the cyclic forces from the valve leaflets. For this reason, a cyclic fatigue loading analysis of the stent is particularly important. Failure resulting from the cyclic forces is an event that could threaten the life of a patient. The frequency of the cyclic forces will be approximately 60 cycles a minute or 31 million cycles a year. If the stent is to have a life of at least ten years, it must be designed to withstand in excess of 310 million loading cycles.

In a recent paper on the fatigue and life prediction of cobalt-chromium stents, a new method is proposed to quantitatively predict the probability of fatigue failure of a stent [25]. This approach combines both a traditional stress-life (S-N) predictive methodology and a fracture mechanics analysis to conservatively evaluate the design life of the stent. The new approach enables the deduction of a safety factor to failure from the simulation data, whereas this safety factor remained unknown in previous methods. The stress-life predictive methodology is of particular interest to this study, however the fracture mechanics analysis is beyond the scope of the present work.

In [25], the processes during stent deployment, namely crimping, balloon-inflation and recoil were first simulated to establish the residual stresses that would be present in the stent after deployment. Thereafter, maximum and minimum pressure loads were then sequentially applied to

the internal surface of the stent to represent the physiological systolic and diastolic blood pressure as a result of the cardiac cycle. The maximum principal stress distribution across the stent for the two pressure loads was subsequently used to calculate a fatigue safety factor (FSF), as described below.

The mean stress and stress amplitude distributions were calculated from the predicted maximum principle stresses across the stent. From these values a modified-Goodman relationship was used to determine a FSF distribution, which basically quantifies the proximity of the mean stress and stress amplitude at any given point to the Goodman curve. The element with the lowest safety factor was then identified as the location most susceptible to fatigue failure.

As the stent that will be developed in the proposed project will be subjected to not only cyclic pressure loads from the cardiac cycle, but also cyclic loads from the valve leaflets, an assessment of the effect of mixed-mode loading would be required.

2.6 Challenges

Due to the unique anatomy of the aortic valve, the percutaneous replacement of this valve presents several distinctive challenges. As the aortic valve lies in close proximity to both the mitral valve and coronary arteries, the correct positioning of the valve is extremely critical. If the valve is to be placed in the native position, inaccurate placement of the valve in either direction could result in severe acute mitral dysfunction or severe acute ischemia. For this reason, alternate strategies towards the positioning of the valve relative to the native position must be carefully considered.

Another challenge posed by percutaneous valve replacement methods is to ensure the stable positioning of the stent in order to prevent migration or embolization, despite high systemic pressures. There also exists a risk of peri-procedural embolization and this aspect must be addressed as well.

Delivery of the prosthesis to the correct position poses a number of difficulties and there are currently two different methods towards the delivery of the prosthesis that are being studied. Both an antegrade and retrograde approach exists towards the delivery of the prosthesis, each with its own advantages and limitations. The transseptal antegrade approach would allow easier passage of large-profile valved stents as well as more precise placement of the prosthesis. However, this approach would entail passage through (and possible damage to) the native mitral valve. The retrograde approach would enable the delivery of the prosthesis without the need for transseptal puncture and would eliminate the risk of damage to the native mitral valve. However, if surgical vascular access and repair is to be avoided, this approach would require a low-profile system.

2.7 Shortcomings

Although a number of papers have been published on the simulation of the processes involved in the implantation of arterial stents, no papers have been found on the simulation of aortic valve stents. For this reason, there is currently no public knowledge available on the forces that these devices are subjected to.

Since percutaneous aortic valve replacement methods have only recently come into practice (past 15 years), there are no published literature on the long-term durability of the valved stent and the risk of late migration or embolization. The valve leaflet material currently used in stented valves are not particularly resistant to corrosion and have a very limited life-span.

Considerable energy is being invested to develop materials in order to enable the effective use of MRI imagery, which is characterized by the ability to display tissue contrast, an absence of radiation and the ability to determine the blood flow within the stent.

Several companies are currently conducting research in the field of percutaneous aortic valve replacement, including NuMed Inc. and Pal-

maz/Bailey. Core Valve is also developing a percutaneously delivered aortic valve system that utilizes a self-expanding stent. Edwards Life-Sciences also researches the development of stented valves and has received FDA (Food and Drug Administration) approval to initiate a clinical trial in patients considered high risk for conventional open-heart valve surgery [26].

2.8 Summary of Knowledge Gained

The following paragraphs provide a summary of the most important knowledge that was gained through the literature review with respect to stent design.

The structural design of the stent is very important with respect to coronary perfusion and the positioning strategy. A short stent is preferable.

The material used to produce a stent must be corrosion resistant, biocompatible and have a high resistance against fatigue. A high elastic modulus and low yield strength is preferable. High tensile properties are required to minimise the profile of the device. A steep work-hardening rate and high ductility is also advantageous.

Seamless tubing is the preferred material for stent applications. Materials with uniform and equally-axed small grain microstructures are preferred with respect to polishing and resistance to fatigue. Metal tubing with extremely tight tolerances are required to ensure an accurate manufacturing process. A smooth surface finish is required to achieve optimal results from the electropolishing process.

The finite element method provides an excellent tool to evaluate stent design parameters, while eliminating the high cost of physically manufacturing many design iterations. A sufficiently sensitive mesh is required to ensure convergence of the solution. For most stent geometries, symmetry models may be used to reduce the analysis time of finite element simulations. The internal pressure load on the stent may be simulated using a three stage continuous linear function.

With respect to stent geometric design, an increase in the number of struts in the circumferential direction has a beneficial effect on radial expansion. An increase in the number of slots in the circumferential direction results in an increase in radial recoil. An increase in strut width provides resistance against excessive elastic recoil as well as an increase in resistance against external compressive forces. However, stent expansion and flexibility are compromised by an increase in strut width.

Fatigue failure is an aspect that should be very carefully addressed during the process of stent design. For this thesis the effect of mixed mode loading on the fatigue life of the stent must be considered.

Delivery and stable stent positioning are challenges which remain largely unsolved and should be addressed during the prosthesis development cycle. A low crimped profile is very important with respect to developing a simple delivery technique.

The knowledge gained in the literature review will serve as a guideline to specify the desired tubing characteristics as well as provide a basis to develop novel strategies towards the geometric design of the stent.

Chapter 3

Stent Design Requirements

3.1 Performance Requirements

A study of the published literature, weekly brain-storming sessions as well as correspondence with Dr. H. Weich, a cardiologist at Tygerberg Hospital, led to the formulation of the performance requirements for the stent. Although an international standard for percutaneous aortic valves does not yet exist, the ISO 5840 International Standard for Cardiac Valve Prostheses [27] was also used as a guideline to formulate the stent design requirements. The identified requirements as well as their accompanying motivations are listed in table 3.1. Along with the motivation, the source of each design requirement (where applicable) is also provided as a reference.

3.2 Material Requirements and Selection

As mentioned in the literature review, the material requirements for a stent used in an aortic valve are corrosion resistance, vascular compatibility, high radial strength, fatigue resistance and visibility using standard X-ray and MRI equipment [20].

There are two distinct material types commonly used for the manufacturing of stents. These include shape-memory alloys and fully an-

Table 3.1: Geometric Design Requirements for the Stent

	Design Requirement	Motivation
a)	Deployed diameter: 20 mm	Average diameter of a sheep's aortic annulus [10]
b)	Maximum length: 16 mm	Minimise profile to avoid coronary obstruction [10]
c)	Crimping diameter: 18 French (6 mm)	Minimise crimping diameter to allow femoral arterial access [10]
d)	Maximum Deployment Pressure: 5 Bar	Maximum realistic deployment pressure for manual pressurisation [10]
e)	Minimum Load Cycles: 156 Million	Load cycles required for a 5-year life-span [27]

nealed bio-metals [20]. Shape memory alloys, such as nitinol, are used to manufacture self-expanding stents whereas bio-metals, such as titanium and cobalt-chrome, are used to manufacture balloon-expandable stents.

Self-expanding stents manufactured from shape-memory alloys have the advantage of a low profile (small minimum crimping diameter), due to the absence of the balloon. The expansion-process of self-expanding stents can also be very well controlled, which is a great advantage for the positioning and deployment process. However, shape-memory alloys are very difficult to machine and handle. Therefore a keen knowledge of the material characteristics and manufacturing experience are required to manipulate them. Another disadvantage of there materials are their limited radial strength. These materials are also fairly expensive.

Bio-metals commonly used in the manufacturing of balloon expandable stents normally have high elastic modules, high tensile properties, a steep work hardening rate and high ductility. As a result of these factors, balloon-expandable stents have high radial strengths and in addition to this, these stents are easy to manufacture and handle. However, the literature indicates that balloon expandable aortic valves are difficult to position and deploy.

In light of the discussion above, it was decided to use a bio-metal to manufacture the stents for this project. The primary motivation for this

selection was the lack of experience working with shape-memory allows, the easy processing and handling of bio-metals as well as the favourable mechanical properties of bio-metals.

With respect to bio-metals, two materials were identified to exhibit properties that are favourable for the manufacturing of the stent prototypes. These materials include Stainless Steel (SS) 316L and the Cobalt-Chrome family of alloys. These two metals have similar mechanical properties, however the cobalt-based alloys exhibit comparatively higher densities, elastic moduli, strengths and differences between yield and ultimate tensile strengths [20]. Although stainless steel is currently the workhorse material used for balloon expandable stents, cobalt-chrome, and specifically CoCr L605 and CoCr MP35N, exhibit slightly superior properties and is becoming more and more popular as materials used in stent manufacturing.

However, cobalt-chrome tubing in the required dimensions is not readily available in South Africa, and on top of this, it is very expensive. As a result of the scarcity and high cost of cobalt-chrome tubing, it was decided that annealed SS 316L would be used to manufacture the stents for this project. Medical grade seamless SS 316L tubing in the required dimensions is also relatively expensive and not readily available. Therefore non-medical grade seam-welded SS 316L was selected as the material for the prototypes. The effects of aspects such as material impurities and tubing concentricity were unknown and would be highlighted by this project. Approximately two meters of tubing with an outer diameter of 9.5 mm and a wall thickness of 0.5 mm were acquired as an off-the-shelf product from a supplier located in the United Kingdom. Ideally, it would be desirable to manufacture the stents to the deployed diameter, however the available laser cutter of Disa Vascular (Pty) Ltd. could only cut to a maximum outer diameter of 10 mm.

In order to verify the mechanical properties of the acquired material, an uni-axial tensile test was conducted on a sample of the material using a 250 kN Amsler machine. The test data was electronically recorded using a SPIDER^{TM} bridge amplifier / data acquisition system and the

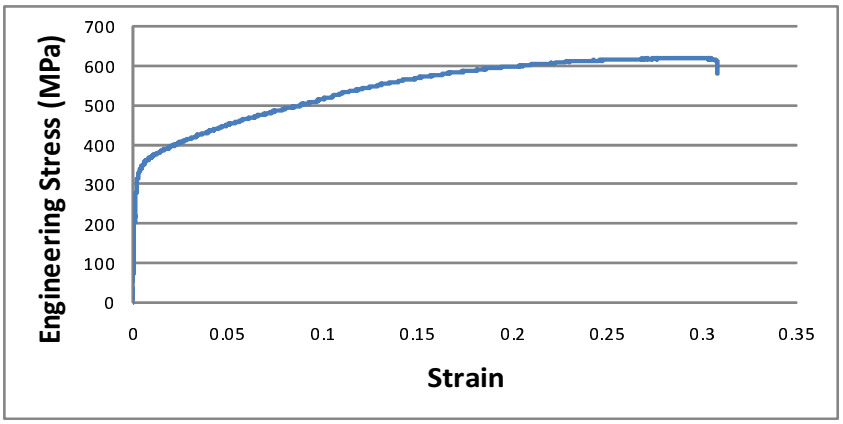

Figure 3.1: SS 316L: Tensile Test

Table 3.2: Mechanical Properties of SS316L

	Literature Data	Experimental Data
Elastic Modulus (E)	193 GPa	187 GPa
Yield Strength	340 MPa	334 MPa
Tensile Strength	670 MPa	619 MPa

results are given in Figure 3.1.

The elastic modulus, yield strength (0.2%) and ultimate tensile strength for the data found in the literature as well as the experimental data are given in Table 3.2.

Since the experimental data corrolated well with the data found in the literature, it was determined that the experimental data would be used in the finite element analyses. The material properties that were determined from the axial test were also used for the circumferencial direction (isotropic material model). This was done because the material was used in the annealed state and it was therefore assumed that the properties in the axial and circumferencial direction would be similar.

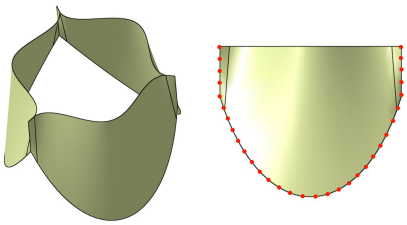

Figure 3.2: Parabolic Assembly

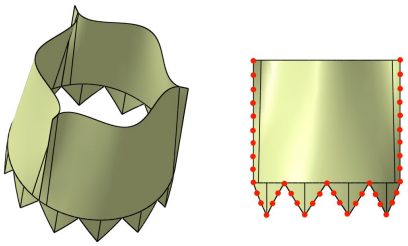

Figure 3.3: Straight Assembly

3.3 Stent-Leaflet Interface Requirements

Mr. A. Smuts, a co-member of the valve development project, determined in his thesis report on the "*Design of Tissue Leaflets for a Percutaneous Aortic Heart Valve*" , that there are two feasible configurations for the shape and the assembly of the valve leaflets to the stent frame [5]. For the first configuration, indicated in Figure 3.2, the valve leaflets are sutured to the stent frame in a parabolic fashion. The line of suturing is indicated by the red dots. This assembly configuration has the advantage that the shape of the valve leaflets represents the profile of the native aortic valve. According to Chikwe et al. [28] this is an important characteristic of an effective replacement valve.

For the second configuration, indicated in Figure 3.3, the valve leaflets have a square form, and the sides of the leaflets are sutured to the stent frame along a straight line. Again, the line of suturing is indicated by the red dots. The advantage of this assembly configuration is the inherent ease of assembly [5].

It was a vital requirement of the stent frame to be compatible with either the parabolic assembly configuration or the straight assembly configuration. For this reason, the stent frame had to have a strut pattern which was orientated in such a manner to allow for the suturing of the valve leaflets along the line of suturing (red dots in the figures).

Table 3.3: Stent Deformation Requirements

	Deformation Process	Initial Diameter (mm)	Final Diameter (mm)
a)	Assembly Expansion	9.5	20
b)	Crimping Process	20	6
c)	Deployment Process	6	20

3.4 Stent Deformation Requirements

It is inevitable that any stent implemented in a percutaneous aortic heart valve would be subjected to a number of deformation processes prior to the final deployment step. As mentioned in Section 3.2, prototype stents for this project would be laser cut from tubing with an outer diameter of 9.5 mm. The stent would therefore be subjected to an initial expansion process, to allow for the valve assembly. The expansion process would be followed by the crimping of the stent on to the balloon catheter. The crimping process, in turn, would be followed by the final deployment process, once the balloon is in position. Details of the required deformation processes are given in Table 3.3. The required changes in diameter during the assembly, crimping and deployment processes were constrained by the design requirements for the stent (refer to Table 3.1).

It was therefore a requirement of the stent that it should be capable of enduring the deformations as described in Table 3.3 without exceeding the material's stress or strain limits.

Chapter 4

Concept Development

4.1 Concept Development Methodology

Since there are no fixed formulas or equations that can be used to determine the required geometry of a stent, the development of a stent requires an iterative concept development phase.

Accordingly, a review of the literature as well as weekly brain-storming sessions aided in the generation of a number of conceptual models, taking into account the design requirements as stated in Chapter 3. Since a complete finite element analysis, to determine all the deformation and performance characteristics of each developed concept, would be extremely time consuming, it was determined that an initial concept evaluation phase would be conducted in which each of the concepts would be subjected to a simplified finite element analysis of the three main deformation processes. The initial finite element analyses are refered to as *"simplified"* as rigid cylinders were used to achieve all of the deformation processes and the stent characteristics such as foreshortening and recoil were not analysed. From these analyses the most promising concepts were selected for an in-depth analysis and concept refinement phase.

For the initial concept evaluation phase, each of the developed concepts were subjected to the initial expansion process, the crimping process and the deployment process by implementing rigid expansion and

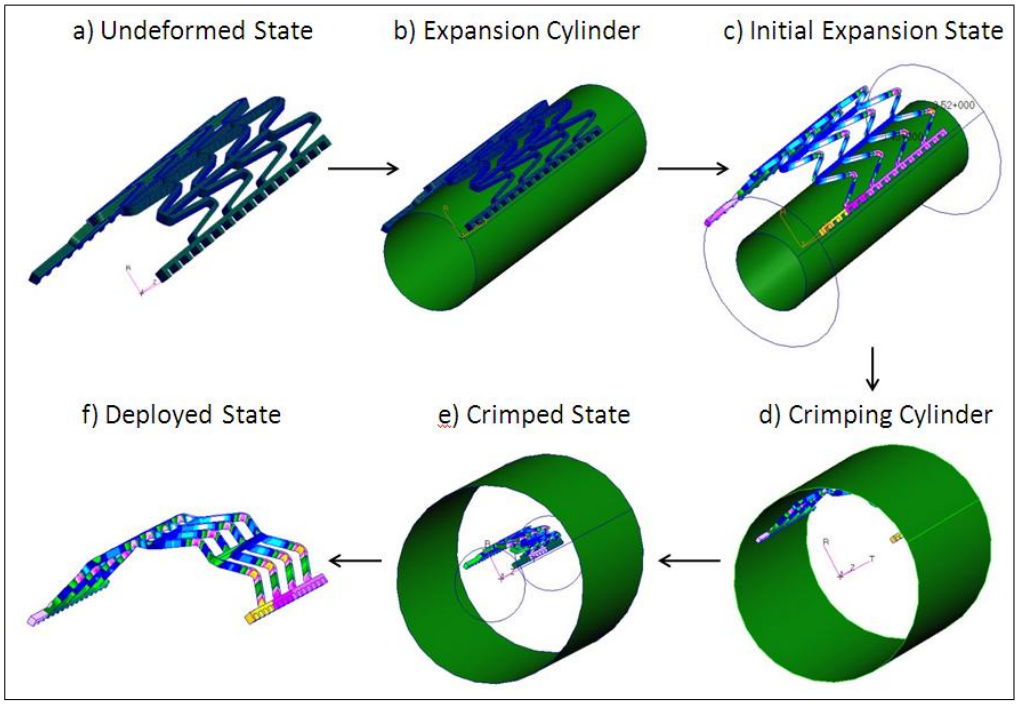

Figure 4.1: FEM Diagram for Concept Simulations

crimping cylinders. An in-depth discussion of the methods and techniques applied to perform the finite element analyses are provided in Chapter 5. Figure 4.1 shows a diagram which depicts the initial expansion (c), crimping (e) and deployment (f) process that was simulated for each concept. For each concept, the stent was first expanded to a diameter of 20 mm, after which the stent was crimped to a diameter of 6 mm. Finally, the stent was again deployed to a diameter of 20 mm.

The concepts which were rejected due to a non-compliance with one or more of the requirements are described in Appendix A.

4.2 Final Conceptual Models

From the initial concept evaluation phase it was concluded that two of the concepts were feasible according to the generated design requirements. These concepts were selected for an in-depth finite element analysis and futher refinement. Figures 4.2 and 4.3 shows the CAD models

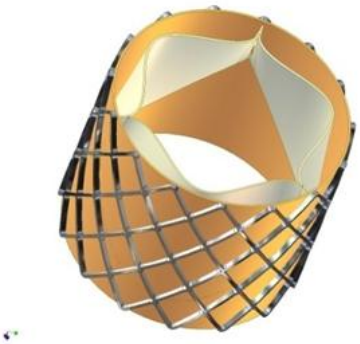

Figure 4.2: Stent Concept A

Figure 4.3: Stent Concept B

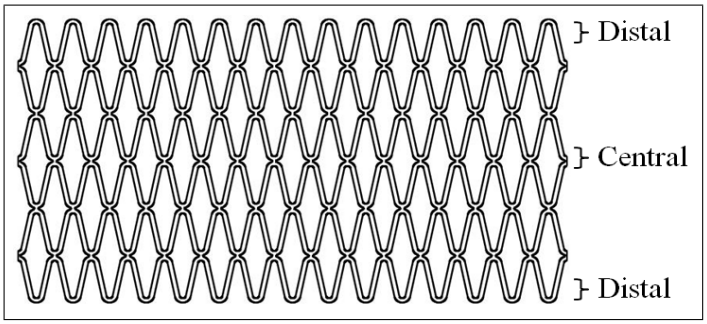

Figure 4.4: Stent Concept A - Wireframe

of the selected concepts as well as the interfaces with the tissue leaflets.

4.2.1 Description of Concept A

Concept A consists of multiple rows of zig-zag shaped struts. The rows are interconnected to each other via conncetions between the apexes and bases of each row of struts. This configuration results in the formation of diamond shaped cells when the stent is deformed into the deployed state (Figure 4.2). This concept is compatible with the parabolic assembly configuration (Section 3.3). Figure 4.4 shows an unfolded wireframe of Concept A. With reference to this text, the distal and central sections of the concept are also indicated in the figure.

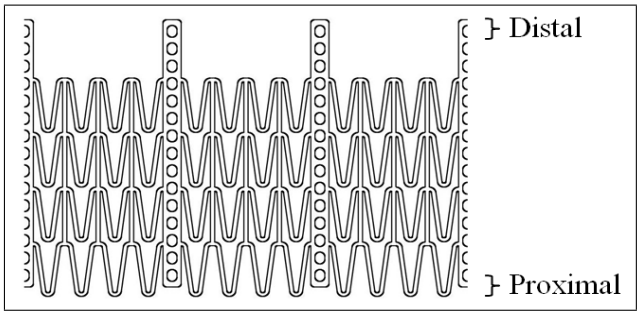

Figure 4.5: Stent Concept B - Wireframe

4.2.2 Description of Concept B

Concept B consists of three support props, which serve as assembly joints for the three leaflets of the valve. The support props are connected with four rows of zig-zag shaped struts, which are translated in the axial direction. This configuration is compatible with the straight assembly configuration (Section 3.3).

Figure 4.5 shows an unfolded wireframe of Concept B. The distal and proximal sections of the concept are also indicated in the figure. This design is similar to the design of the stent used in the Edwards SAPIEN Transcatheter Heart Valve from Edwards Life Sciences [29], however, there are some critical differences. The support props extend well beyond the end of the struts, whereas, the Edwards design has support props which end in line with the struts. This feature was implemented to allow for the straight assembly configuration, while minimising the possibility of coronary obstruction. The rows of the zig-zag strut pattern are uni-directional (they face in the same direction), whereas the zig-zag strut pattern of the Edwards valve are mirrored around the midplane of the stent. The uni-directional strut configuration helps to minimise the cyclic stresses to which the extended support props would be subjected (Section 5.8). This may be attributed to the fact that the top row of struts are connected with their top end to the support props, as opposed to the support props extending to the bottom ends of the top row of struts, which is the case with the Edwards design.

Chapter 5

Numerical Simulations

5.1 Introduction

Although the two most promising stent concepts were identified as described in Section 4.2, the exact geometric dimensions that would be most suited for the specific stent application had to be determined. For this reason an in-depth FEA was conducted for each concept to determine the influence of strut width on the stent characteristics such as stress and strain, recoil, foreshortening, fatigue-life, etc. To eliminate possible ambiguity between strut width and strut thickness, Figure 5.1 shows a section of Concept A for which the strut width is indicated. Strut thickness is determined by the wall thickness of the tubing used to manufacture the stent.

For Concept A, the analyses were conducted for strut widths of 0.20 mm, 0.23 mm, 0.25 mm and 0.27 mm. For Concept B, the analyses were conducted for strut widths of 0.20 mm, 0.22 mm, 0.25 mm and 0.27 mm.

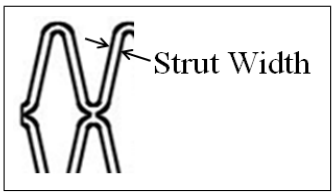

Figure 5.1: Strut Width

Table 5.1: Concept A: Geometric Parameters

Category	Strut Width			
	.20 mm	.23 mm	.25 mm	.27 mm
Metal surface area (mm^2)	128.559	137.354	141.115	143.877
Stent surface area (mm^2)	562.427	569.163	572.276	575.862
Metal-Surface area ratio	0.229	0.241	0.247	0.250
Undeformed length (mm)	18.845	19.071	19.175	19.295
Deployed length (mm)	17.499	17.635	17.729	17.941

There is no scientific reason for the discrepency between a strut width of 0.23 mm used for Concept A, and 0.22 mm used for Concept B, whereas the other width values are the same. This was due to a technical error made during the CAD modelling of Concept B, which was discovered at a stage which was too late to remodel, simulate and process the results for a strut width of 0.23 mm. Since the data for a strut width of 0.22 mm was still usefull to provide insight into the stent behaviour, it was included in the thesis.

For both concepts, the geometric parameters for the various strut widths are given in Tables 5.1 and 5.2. With respect to the tables, "metal surface area" refers to the outer surface area of the stent, whereas "stent surface area" refers to the arterial surface area covered by the stent (stent circumference $\times$ stent length). The geometric parameters for the concepts were determined from the generated CAD models. From the numerical analyses a strut width could be selected for each concept that would be most suited for the application. The results of the analyses are reported in this chapter.

5.2 Analysis of Stent Loading Conditions

Prior to performing a finite element analysis of the stent loading and deformation conditions, the processes involved during the assembly, deployment and operation of a percutaneous aortic heart valve need to be addressed.

Table 5.2: Concept B: Geometric Parameters

Category	Strut Width			
	.20 mm	.22 mm	.25 mm	.27 mm
Metal surface area (mm^2)	150.384	159.235	172.838	182.000
Stent surface area (mm^2)	515.574	516.171	517.066	517.663
Metal-Surface area ratio	0.292	0.308	0.334	0.352
Undeformed length (mm)	20.5	20.5	20.5	20.5
Deployed length (mm)	20.5	20.5	20.5	20.5

The stent is first mechanically expanded from the manufactured diameter to the final deployed diameter in order to allow for the assembly of the valve leaflets to the stent. The assembled prosthesis is then loaded onto a balloon catheter. For this step, the stent is temporarily crimped onto the inflatable balloon portion of the catheter, forming the intra-vascular stent delivery system. Thereafter the delivery system is percutaneously inserted into the femoral artery where it is translated along the anatomical pathways leading to the position of the native aortic valve (Figure 5.2). Once in the desired position, deployment of the prosthesis is accomplished by the inflation of the balloon via hydraulic pressurisation. This results in the expansion of the prosthesis into the targeted site. During this step, the native aortic valve becomes trapped between the stent and the wall of the aortic sinuses. Upon reaching the desired deployment diameter, the balloon catheter is removed by deflation of the balloon and subsequent extraction of the delivery system. The final step of the deployment procedure occurs when the stent elastically recoils to a slightly smaller diameter.

The deployment process is followed by the onset of a continuous cyclic loading process which is induced by the cyclic leaflet forces as well as the cyclic systolic and diastolic pressurisation. Both the cyclic leaflet forces as well as the cyclic pressurisation is caused by the cardiac heartbeats.

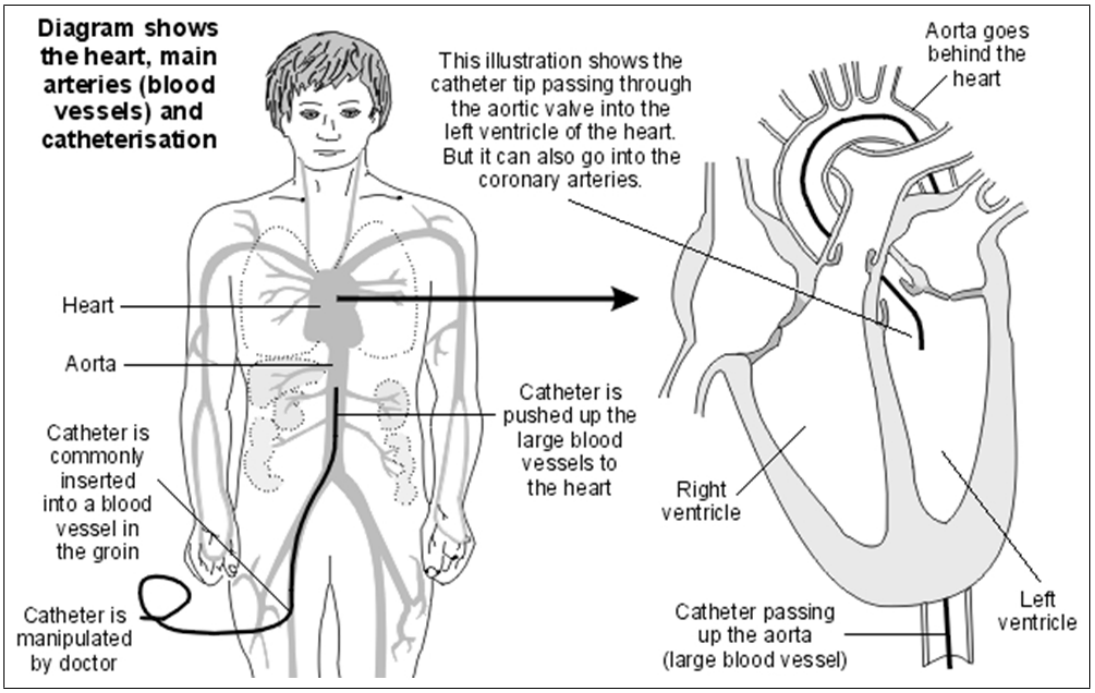

Figure 5.2: Anatomical Vascular Pathways Leading to Native Aortic Valve [3]

5.3 Simulation Environment Setup

The FE simulation of the stent concepts presented a complex problem as it involved severe non-linear behavior. The non-linear behavior included geometric, contact and material non-linearities. The geometric non-linearity was accounted for by activating the large stain/large displacement algorithm and the material non-linearity was accounted for by implementing a *true stress - true strain* elastic-plastic material model with isotropic hardening. Contact boundary conditions were imposed to manage the contact non-linearities (Section 5.5.2). In order to ensure that the non-linear problem converged to an accurate state of equilibrium, residual force and displacement tolerances of 1% were activated.

Adaptive time stepping was used along with the Full Newton Raphson iterative method to ensure that the iterative correction of the equilibrium state could take place. A time-step scale of 1.5 was implemented and the target iterations per increment was set to 15. A Multi-Frontal (Di-

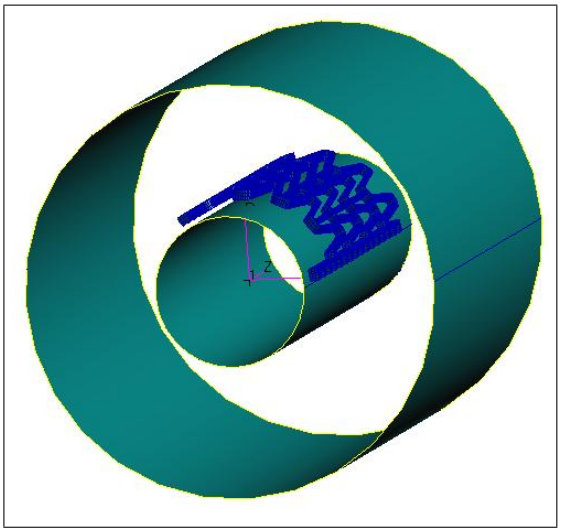

Figure 5.3: Concept B: FEM Model Setup

rect) Sparse solver was implemented to solve the equilibrium equations.

5.4 Finite Element Models of the Stent Concepts

To set up the numerical models for the loading conditions as described in Section 5.2, both stent concepts were first modeled as bi-parametric surfaces using a CAD package. The surfaces were then imported into the pre-processor MSC.Patran where they were first meshed using quadratic surface elements. The surface elements were subsequently extruded to eight-noded, isoparametric, three-dimensional brick elements with tri-linear interpolation [30].

To simulate the "rigid" crimping and expansion of the stents, two cylinders were created on either side of the stents using semi-rigid surfaces. Figure 5.3 shows the model setup that was used for the modeling of Concept B. The model setup of Concept A was similar.

5.5 Boundary Conditions

5.5.1 Displacement Constraints

Because of the cyclic symmetric forces imposed by the valve leaflets during the fatigue loading step as well as the cyclic symmetry about the longitudinal axis present in both stent models, it was not necessary to model the entire stent body, but rather only the segment of each stent that would be subjected to the cyclically repeating forces. Since the valve leaflet forces are tri-cyclically symmetric (each of the leaflets imposes forces on the stent of the same magnitude and direction) it was only required to model one third for both concepts.

For both concepts, the nodes in the planes of cyclic symmetry were constrained to only allow for axial and radial translation in the symmetry planes. For Concept A (Figure 4.2), axial constraints were imposed on a single node in the plane of symmetry along the longitudinal axis (center nodes) to prevent rigid body translation, ensuring that the model was fully constrained within the simulated environment. The nodes at either end of the stent was left unconstrained to allow for the extension or shortening of the stent during the load steps. The imposed displacement constraints for Concept A are indicated in Figure B.1 of Appendix B. For Concept B (Figure 4.3), axial constraints were applied to a single node at one end of the stent, while the other end was left free to extend or shorten during the load steps. This was done to prevent the rigid body translation of the stent, also ensuring that the model was fully constrained within the simulated environment. The imposed displacement constraints for Concept B are indicated in Figure B.2 of Appendix B.

For both concepts, the maximum displacement of all the nodes were constrained to simulate the displacement constraint imposed by the nominal deployment diameter of the balloon. This implied that none of the nodes could exceed the deployed diameter of 20 mm.

5.5.2 Contact Constraints

For both stent models, rigid-deformable contact constraints were established between the inner and outer surfaces of the stents and the semi-rigid crimping and expansion cylinders. Self-contact were also activated for the stent models. Elderly patients who qualify for a percutaneous aortic valve replacement will most likely have aortic annuli and aortic valve leaflets which are severely calcified. As a result of this, the geometry of the calcified tissue may vary greatly between patients. On top of this, the material properties of the calcified tissue are unknown and difficult to determine. It is also likely that the calcified material would be fairly brittle and have a limited contribution to the radial recoil of the stent. For these reasons the interaction (contact) between the stent and the external environment were not simulated for the purpose of this project.

5.6 Loadings Conditions

The loading conditions for the concepts were modeled as a number of discrete steps in the sequence as they would occur during service. These steps include (i) assembly expansion, (ii) crimping, (iii) balloon-deployment, (iv) elastic recoil and (v) cyclic loading of the deployed stent. A representative of ESTEQ Engineering suggested that a solution time of one second would be sufficient for each of the large deformation steps to allow for convergence to the quasi-equilibrium state [31]. A solution time of 0.5 seconds was also deemed sufficient for the elastic recoil step. The solution time for each step is indicated in Table 5.3.

The initial assembly expansion step was simulated by applying a time-field growth factor to the semi-rigid expansion cylinder. This implies that the diameter of the expansion cylinder was controlled using a time dependent table. Since a rigid-deformable contact constraint was active, the stent expanded along with the expanding cylinder to the desired diameter. After the expansion step, the crimping step was similarly accom-

Table 5.3: Load Steps: Solution Time

Time (sec)	Load Step
0 - 1	Assembly Expansion
1 - 2	Crimping
2 - 3	Balloon-Deployment
3 - 3.5	Elastic Recoil
3.5 - 4.5	Cyclic Loading

plished by applying a negative time-field growth factor to the semi-rigid crimping cylinder.

The balloons used in stent applications are often modeled using a hyperelastic Mooney-Rivlin material model [32]. A hyperelastic material is difficult to model since the material may experience a strain which is several orders of magnitude higher compared to traditional materials, which increases the structural instability of the elements [33]. In practice, balloons used for stent applications are manufactured from polyester polyethylene terephthalate (PET) materials which are non-compliant or low-compliant [34]. This implies that the balloons retain their designed shape even under high pressure. An attempt was made to model the balloon according to the Mooney-Rivlin material model, however, it was found that this model does not accurately describe the behavior of a PET balloon.

Since an appropriate model could not be found or be generated to model a PET balloon, it was decided to model the balloon-deployment step by applying a uniform pressure to the internal surface of the stent. The pressure was linearly increased until the stent reached the desired deployed diameter. This approach had the limitation that the transfer of outward vectored forces from the bulging balloon membrane to the stent was not taken into account. Snapshots of some intermediate iterations of the assembly, crimping and deployment load steps for Concept B can be found in Appendix C.

After the deployment step, the stents were allowed to recoil by linearly decreasing the internal surface pressure. This load step represented

Table 5.4: Concept A: Mesh Convergence Analysis

# Nodes	# Elements	Deployed Diameter (mm)
5640	1880	19.92
26050	13760	16.9
61200	37850	17.42
103200	68400	17.5
230580	169760	17.7

the deflation of the balloon and the retraction of the balloon catheter.

The final cyclic load step was constructed to represent the physiological systolic and diastolic blood-pressure loads as well as the cyclic forces exerted by the valve leaflets. This load step is described in more detail in Section 5.8.

5.7 Analysis of Numerical Results

5.7.1 Mesh Convergence Analysis

In order to characterise the mesh sensitivity of the analyses and ensure that an adequately sensitive mesh would be used, a simple deployment analysis was conducted for both stent models. Linearly increasing pressures of 0.0 - 1.25 MPa and 0.0 - 0.43 MPa were respectively applied to the internal surfaces of Concept A and Concept B. This analysis was conducted with various mesh sizes and the deviation in the deployed diameter was compared with the variation in mesh size. The results for Concept A and Concept B are displayed in Table 5.4 and Table 5.5 respectively.

From the results given in Table 5.4 and Table 5.5, it can be seen that, for Concept A, the difference between the deployed diameter for 61200 nodes and 230580 nodes was about 1.61%. 61200 nodes corresponded to three elements along the width of the struts and five elements along

Table 5.5: Concept B: Mesh Convergence Analysis

# Nodes	# Elements	Deployed Diameter (mm)
7452	2612	22.22
29080	15696	16.6
71388	45190	17.64
118608	79890	17.72
140328	96450	17.76

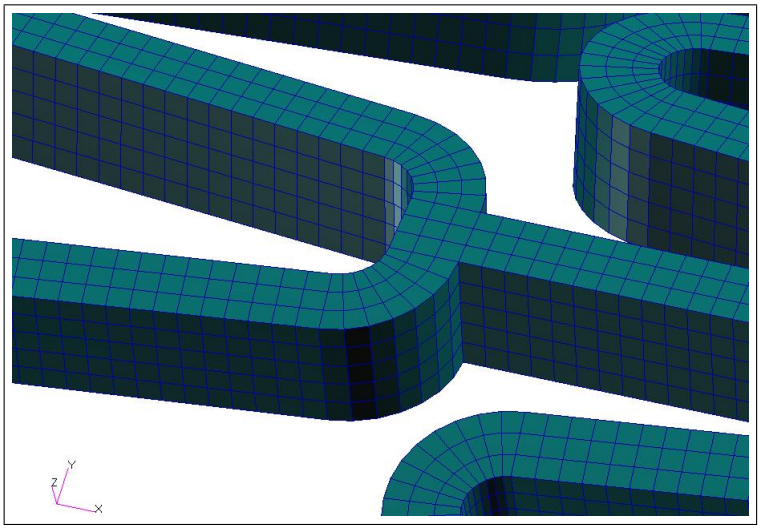

Figure 5.4: Concept B: Mesh Configuration

the thickness of the struts. For Concept B, the difference between the deployed diameter for 71388 nodes and 140328 nodes was about 0.7%. 71388 nodes also corresponded to three elements along the width of the struts and five elements along the thickness of the struts. Thus, to reduce the analysis time, while maintaining accurate results, the simulations for both concepts were conducted with a mesh which corresponds to three elements along the width of the struts and five elements along the thickness of the struts. As an example of this configuration a section of the finite element model used for Concept B is shown in Figure 5.4.

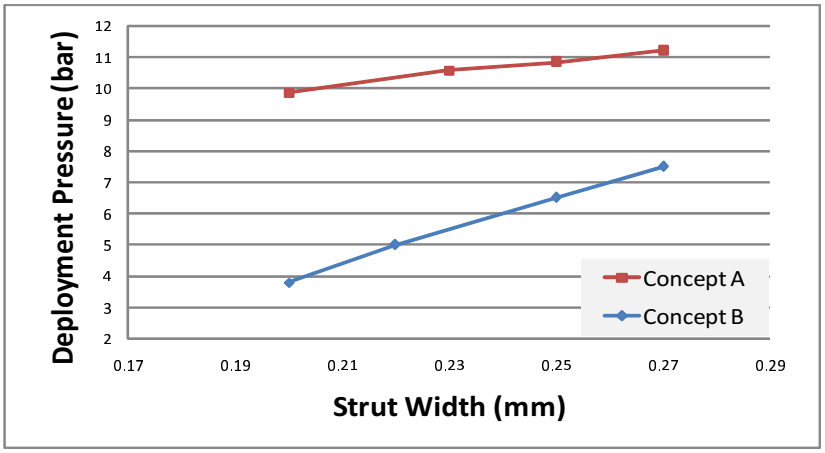

Figure 5.5: Strut Thickness vs. Deployment Pressure

5.7.2 Effect of Strut Width on Radial Strength

As mentioned, the width of a stent's struts in the circumferential direction has an influence on certain important characteristics of the stent, such as stent profile, referring to the minimum crimp diameter, and radial strength. A number of simulations were conducted for the selected concepts to investigate the influence of the variation in strut width on the radial strength of the stents. For these simulations, the initial expansion process, crimping process and deployment to the functional diameter were simulated for the strut widths as mentioned in Section 5.1. The required pressure to achieve the functional diameter were recorded against the variation in strut widths. Figure 5.5 displays a plot of the strut width vs. the deployment pressure for both concepts.

From the figure it can be seen that both stent concepts display a more or less linear relationship between the strut width and the required deployment pressure. It is notable that Concept A requires a substantially larger deployment pressure compared to Concept B. It can also be seen that, in the case of Concept B, the deployment pressure displays a higher sensitivity to a variation in strut width.

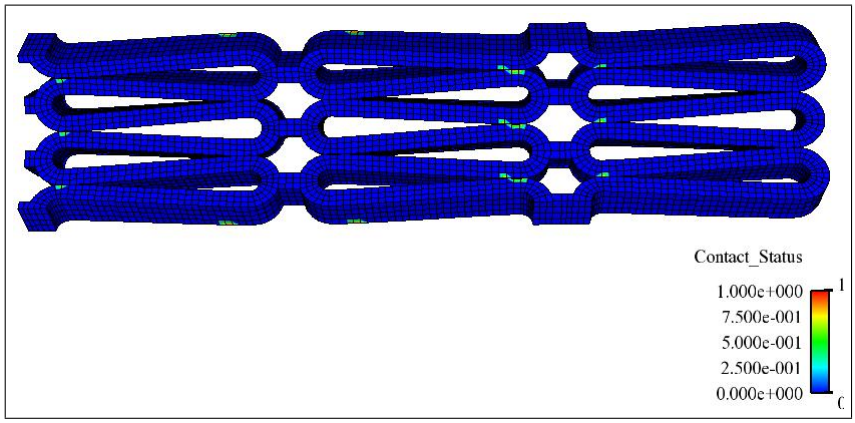

Figure 5.6: Concept A: Minimum Crimped Diameter

5.7.3 Minimum Crimp Diameter

From the literature review it was determined that the crimped profile of a percutaneous aortic valve plays a major role in the performance of the device as it is directly related to the ease at which the device may be guided through the arterial pathways of the body. It is therefore desirable for the device to exhibit the minimum possible crimped profile. Since the crimped profile of the device is directly related to the minimum possible crimped profile of the stent component, simulations were conducted to determine the relationship between the variation in strut width and the minimum achievable crimped diameter for each concept. For the simulations, stents with different strut widths were crimped with a rigid cylinder to the minimum allowable crimped diameter - which was defined as the diameter at which adjacent struts came into contact. The minimum allowable crimped diameters for each concept are indicated in Figure 5.6 and Figure 5.7. The areas of the struts that are in contact are also indicated by the color spectrum.

The minimum crimped diameter for the different strut widths were recorded and are displayed on the plot in Figure 5.8. From the figure it can be seen that, for each concept, there exists a linear relationship between the variation in the strut width and the minimum crimp diameter. It can also be seen that, for comparable strut widths, Concept A exhibits

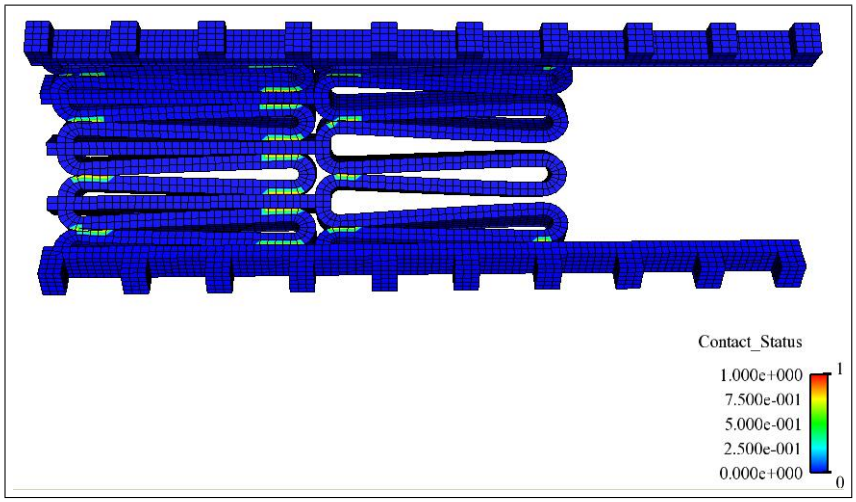

Figure 5.7: Concept B: Minimum Crimped Diameter

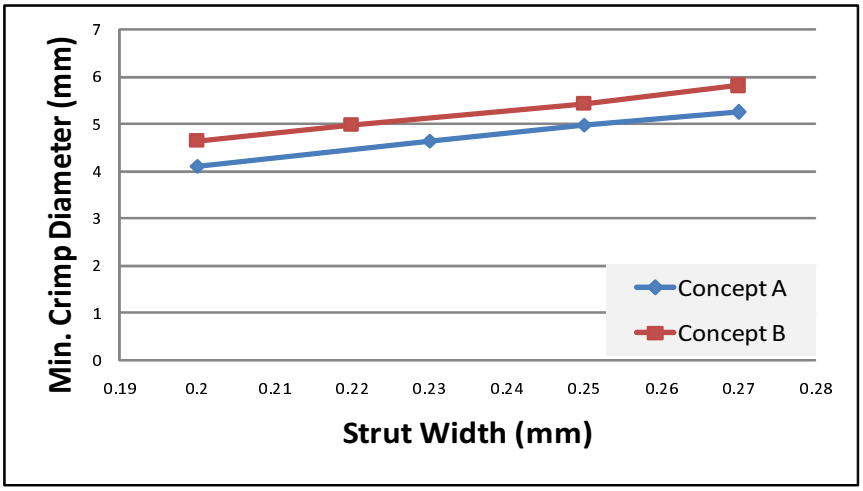

Figure 5.8: Strut Width vs. Minimum Crimp Diameter

a slightly smaller crimped diameter. It should be noted that ultimately the minimum possible crimped diameter of the assembled device will be restricted by the valve leaflets, which will be assembled to the inside of the stent, as well as the profile of the deployment balloon. Nevertheless, the analysis was useful to indicate how each concept performed under the crimping process as well as how the variation in strut width affected the minimum possible crimped diameter.

5.7.4 Analysis of Accumulated Stress and Strain

The software package CEI Ensight 8.2 was used to post-process the FEM data generated by the simulations and extract the maximum true stresses and strains across the stents for each increment of the assembly, crimping and deployment load steps. Figures 5.9 and 5.10 show plots of the maximum true stresses induced in both concepts during the simulated load steps. The true stress measure accounts for changes in the cross sectional area by using the instantaneous values for areas, as opposed to engineering stress which uses the fixed undeformed cross-sectional area as a reference. The true stress measure provides a more accurate measurement for events such as large deformations.

In Figures 5.9 and 5.10 the results for stents with different strut widths are compared. For purposes of clarity the results for a strut width of 0.2 mm has been excluded for both concepts. From the figures it can be seen that, for both concepts, the maximum induced stresses increase with an increase in strut width. The effect of accumulated stress is also clearly visible from the plots. For both concepts, it is important to evaluate the safety factors against failure with respect to the true ultimate strength of the material, which is 965 MPa. The safety factors against failure as a function of strut width is given in Table 5.6. From the table it can be seen that, for both concepts, the maximum induced true stress does not exceed the true ultimate strength for any of the strut widths.

Figures 5.11 and 5.12 show plots of the maximum true plastic strain induced in both stent concepts during the simulated load steps. Again, in each plot the results for stents with different strut widths are compared. For purposes of clarity the results for a strut width of 0.2 mm has been excluded for both concepts. The effect of accumulated plastic strain is also clearly visible from the plots. For both concepts, it is important to evaluate the safety factors against failure with respect to the fracture strain of the material, which is 0.48 or 48% [20]. The safety factors against strain failure as a function of strut width is given in Table 5.7. From the

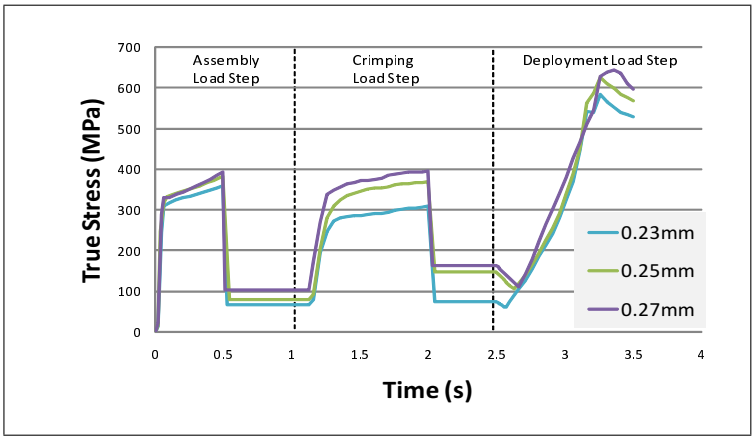

Figure 5.9: Concept A: True Stress vs. Time

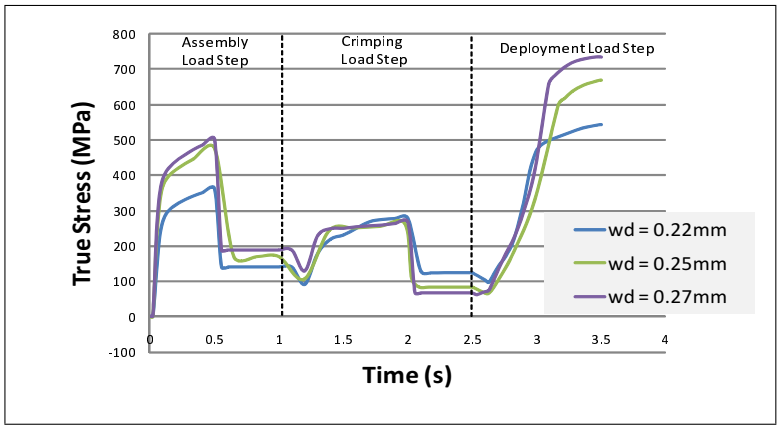

Figure 5.10: Concept B: True Stress vs. Time

Table 5.6: Safety Factors against Stress Failure

	Strut Width			
	.20 mm	.23 mm	.25 mm	.27 mm
Concept A	1.80	1.65	1.54	1.50
	.20 mm	.22 mm	.25 mm	.27 mm
Concept B	1.77	1.75	1.44	1.37

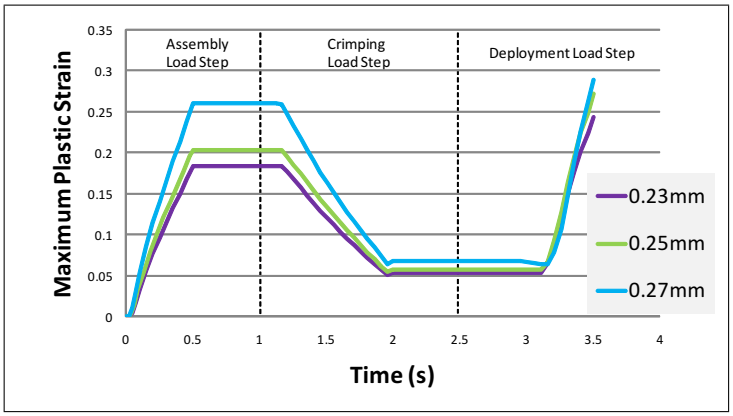

Figure 5.11: Concept A: True Strain vs. Time

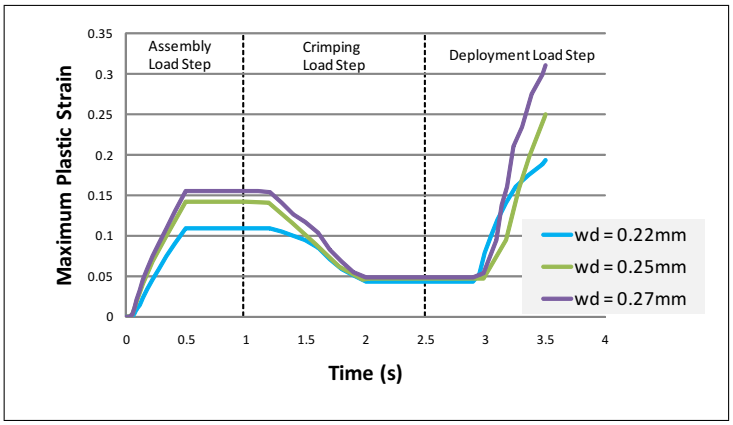

Figure 5.12: Concept B: True Strain vs. Time

Table 5.7: Safety Factors against Strain Failure

	Strut Width			
	.2 mm	.23 mm	.25 mm	.27 mm
Concept A	2.29	1.97	1.77	1.66
	.20 mm	.22 mm	.25 mm	.27 mm
Concept B	2.53	2.49	1.92	1.55

table it can be seen that, for both concepts, the maximum induced plastic strain does not exceed the fracture strain for any of the strut widths.

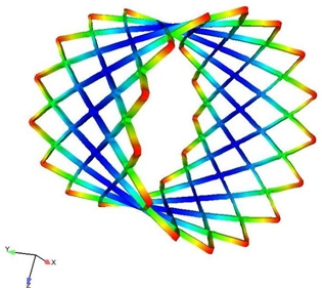

Figure 5.13: Concept A: Dog-boning

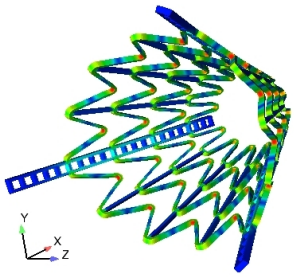

Figure 5.14: Concept B: Coning

5.7.5 Deployment Characteristics

Deployment characteristics refer to the modes by which the stent concepts deform during the deployment load step. These characteristics include modes of deformation, foreshortening and elastic recoil. An analysis of these characteristics are valuable to the designer as they help to characterise the expected behavior of the concepts during deployment.

5.7.5.1 Mode of Deformation

The mode of deformation refers to the manner by which the concepts deform from the crimped state to the deployed state. Figures 5.13 and 5.14 show the intermediate deformation states of Concept A and Concept B during the deployment load step.

From Figure 5.13 it can seen that Concept A conforms to a "dog-boning" deformation mode. The parameter that was defined to describe the state of dog-boning during the deployment load step is given in Equation 5.7.1.

$$Dog - boning = \frac{D^{load}_{distal} - D^{load}_{central}}{D^{load}_{distal}} \tag{5.7.1}$$

D^{load}_{distal} is the instantaneous diameter at the distal end of the stent and $D^{load}_{central}$ is the instantaneous diameter at the center of the stent. Figure 5.15 shows the defined "dog-boning" parameter as a function of the stent

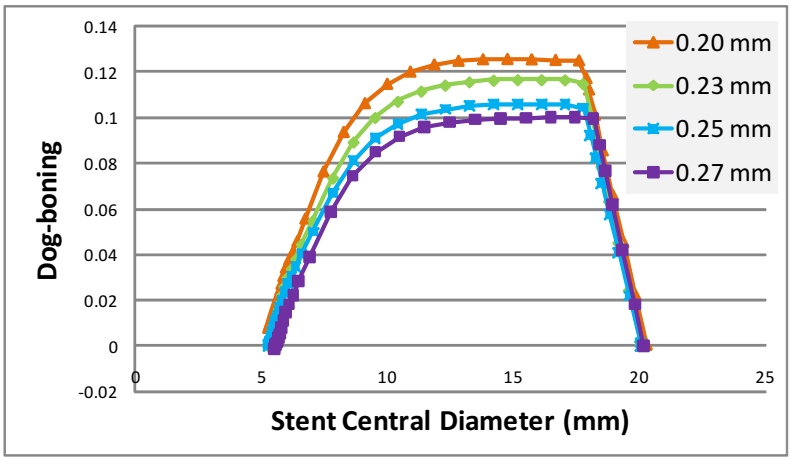

Figure 5.15: Concept A: Dog-boning vs. Central Outer Diameter

central outer diameter for the various strut widths. From the figure it can be seen that dog-boning of the stent decreases slightly with an increase in strut width.

It is also evident that the amount of dog-boning decreases linearly to zero during the final stage of the deployment load step. This happens as the central nodes catch up with the distal nodes, which have already reached the predefined displacement constraint (see Section 5.5.1 for a rationalisation of the deployment constraints placed on the outer nodes). The phenomenon of a decreases in dog-boning during the final stage of deployment also happens in practice (see Section 7.2.3).

From Figure 5.14 it can seen that Concept B conforms to a "coning" deformation mode. The parameter that was defined to describe the coning mode of deformation is given in Equation 5.7.2.

$$Coning = \frac{D^{load}_{distal} - D^{load}_{proximal}}{D^{load}_{distal}} \tag{5.7.2}$$

Again, D^{load}_{distal} is the instantaneous diameter at the distal end of the stent and $D^{load}_{proximal}$ is the instantaneous diameter at the proximal end of the stent. Figure 5.16 shows the defined "coning" parameter as a function of the stent proximal outer diameter. For clarity purposes the results of Concept B for a strut width of 0.20 mm was not included in the graph.

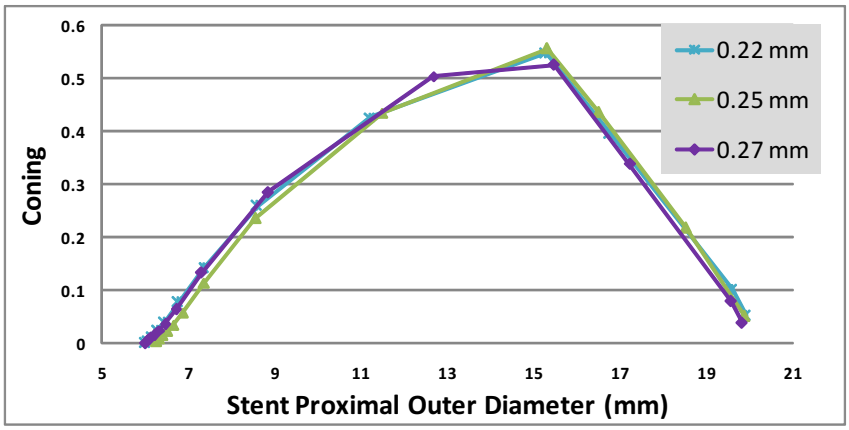

Figure 5.16: Concept B: Coning vs. Outer Diameter

From the figure it can be seen that the level of coning is not dependent on the strut width of the stent.

5.7.5.2 Elastic Recoil

As mentioned in Section 1.4, elastic recoil refers to the elastic spring-back of the stent after the deployment pressure has been removed. As mentioned in Section 5.6, after the deployment load step, the internal pressure on the stent models was linearly decreased to allow for elastic recoil to take place. Two recoil parameters were defined, namely longitudinal recoil and radial recoil. These parameters are described by Equations 5.7.3 and 5.7.4. It should be noted that, for Concept B, longitudinal recoil was defined for the length of the stent containing struts, ignoring the three support props which does not experience a change in length.

$$LongitudinalRecoil = \frac{L^{load} - L^{unload}}{L^{load}} \tag{5.7.3}$$

L^{load} is the longitudinal length before load removal and L^{unload} is the longitudinal length after load removal.

$$RadialRecoil = \frac{D^{load} - D^{unload}}{D^{load}} \tag{5.7.4}$$

D^{load} is the outer diameter before load removal and D^{unload} is the

Table 5.8: Concept A: Recoil Analyses

SW (mm)	L^{load} (mm)	L^{unload} (mm)	D^{load} (mm)	D^{unload} (mm)	Longitudinal Recoil (%)	Radial Recoil (%)
0.20	17.499	17.635	20	18.791	-0.777	6.047
0.23	17.600	17.729	20	18.894	-0.733	5.53
0.25	17.818	17.941	20	18.877	-0.690	5.613
0.27	17.836	17.957	20	19.054	-0.678	4.730

Table 5.9: Concept B: Recoil Analyses

SW (mm)	L^{load} (mm)	L^{unload} (mm)	D^{load} (mm)	D^{unload} (mm)	Longitudinal Recoil (%)	Radial Recoil (%)
0.20	16.414	16.443	20	18.488	-0.175	7.557
0.22	16.397	16.512	20	18.689	-0.702	6.557
0.25	16.424	16.515	20	18.7398	-0.554	6.301
0.27	16.461	16.532	20	18.801	-0.431	5.995

outer diameter after load removal. Recoil analyses were conducted for both concepts to determine the effect of a variation of strut width on the recoil parameters. The results of these analyses are given in Table 5.8 and 5.9. From the analyses it can be seen that the magnitude of the longitudinal recoil parameters for Concept A are in the same range as those of Concept B. It is also evident that, for both concepts, the longitudinal recoil decreases slightly with an increase in strut width. Both concepts also exhibit radial recoil parameters of similar magnitude and radial recoil decreases slightly with an increase in strut width.

5.7.5.3 Foreshortening

Foreshortening is defined as the amount by which a stent shortens, along the longitudinal axis of the stent, during the deployment load step. The equation that was used to describe the parameter for foreshortening is given in Equation 5.7.5. It should be noted that, for Concept B, foreshortening was defined for the length of the stent containing struts, ignoring the three support props which did not experience a change in length.

Table 5.10: Foreshortening Analyses

Concept	SW (mm)	L^{crimp} (mm)	L^{final} (mm)	Foreshortening (%)
A	0.20	19.265	17.635	8.461
	0.23	19.411	17.729	8.665
	0.25	19.601	17.941	8.469
	0.27	19.718	17.957	8.931
B	0.20	17.195	16.443	4.374
	0.22	17.202	16.512	4.013
	0.25	17.204	16.515	4.004
	0.27	17.199	16.532	3.879

$$Foreshortening = \frac{L^{crimp} - L^{final}}{L^{crimp}} \tag{5.7.5}$$

L^{crimp} is the crimped longitudinal length of the stent and L^{final} is the final deployed longitudinal length of the stent. Foreshortening analyses were conducted for both concepts to determine the effect of a variation of strut width on the foreshortening parameter. The results of these analyses are given in Table 5.10. From the table it can be seen that, for both concepts, foreshortening is not influenced significantly by a variation in strut width. It is noteworthy that Concept A displays almost twice the amount of foreshortening, compared to Concept B.

5.8 Stent Fatigue Analysis

Once the assembled valve is deployed into the desired position relative to the native aortic valve, the stent component will be subjected to cyclic loads as a result of the cyclic systolic and diastolic blood pressure as well as the cyclic leaflet forces. For both concepts, a fatigue-life FEM analysis was conducted to assess the relationship between the fatigue-life and the strut width. A stress-life (S-N) analysis approach in combination with the Modified Goodman Failure Criteria was selected as the methodology that would be followed to perform the analyses [35; 36].

The Modified Goodman Failure Criteria is a method used to plot the midrange and alternating stresses against a predefined failure criterion, known as the Modified Goodman Line. This method is often used for analysis and design applications and is ideal for our application as it may be easily graphed, it provides insight into the fatigue problem and the answers may be scaled from the diagram as a check on the algebra.

5.8.1 Analysis of the Fatigue Loads

In order to perform the stress-life analysis for fatigue loading, the governing fatigue loads had to be analysed. In a thesis report by Van Aswegen on the *Dynamic Modeling of a Stented Aortic Valve*, the effect of the dynamic pressure difference across the valve on the forces exerted by the valve leaflets were analysed [4]. In the paper a worst case scenario was investigated with a maximum pressure difference of 180 mmHg. Figure 5.17 shows the resulting dynamic pressure that was recorded, by a fluid-structure analysis, on the aortic side of the valve. The total resultant reaction forces exerted by the valve leaflets during a single cardiac cycle were also analysed in the thesis and the results are given in Figure 5.18. The simulation was conducted for a heart rate of 60 bpm. Since it was possible to formulate a symmetry-solution problem, only half of a single leaflet was simulated. The simulation indicated that the maximum radial force exerted by a single valve leaflet is 1.7 N, while the maximum axial force exerted is 1.74 N. In a thesis report by Smuts on the *Investigation of Tissue Materials for Implementation in a Percutaneous Aortic Heart Valve*, the distribution of the valve leaflet reaction forces were simulated using FEM [5]. The result of this simulation indicated that approximately 37% of the total reaction forces were concentrated at the top of the valve leaflet, while the remaining component of the reaction forces were more or less evenly distributed along the rim of the leaflet. For this thesis, only the parabolic assembly configuration was considered with respect to the fatigue analysis as both assembly configurations appeared to exert similar reaction forces. The results of the FEM analysis conducted by Smuts

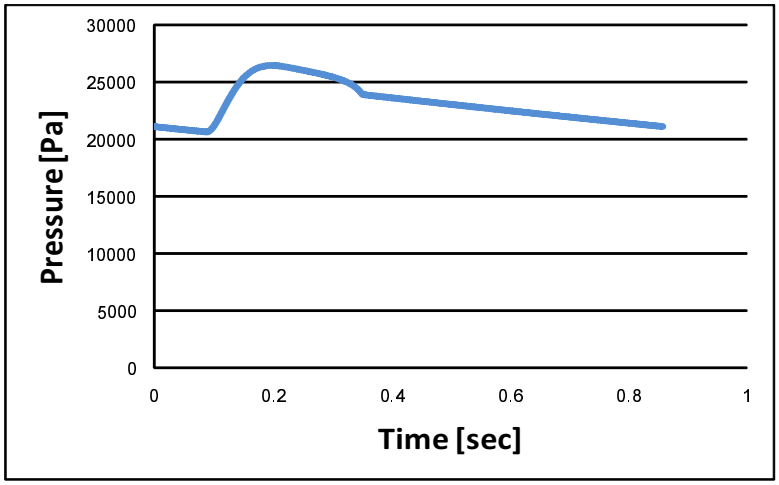

Figure 5.17: Dynamic Pressure Difference Across Aortic Valve [4]

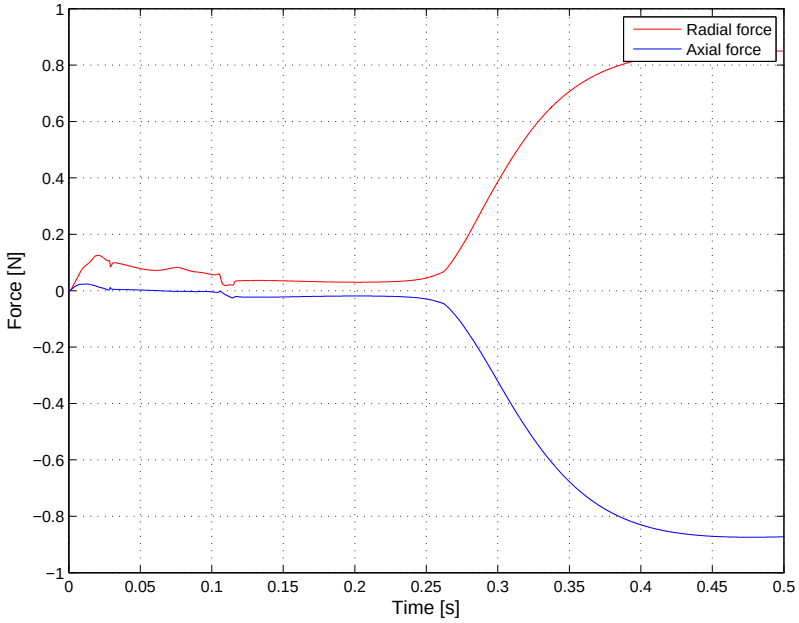

Figure 5.18: Valve Leaflet Force for a Half Leaflet [4]

are indicated in Figure 5.19.

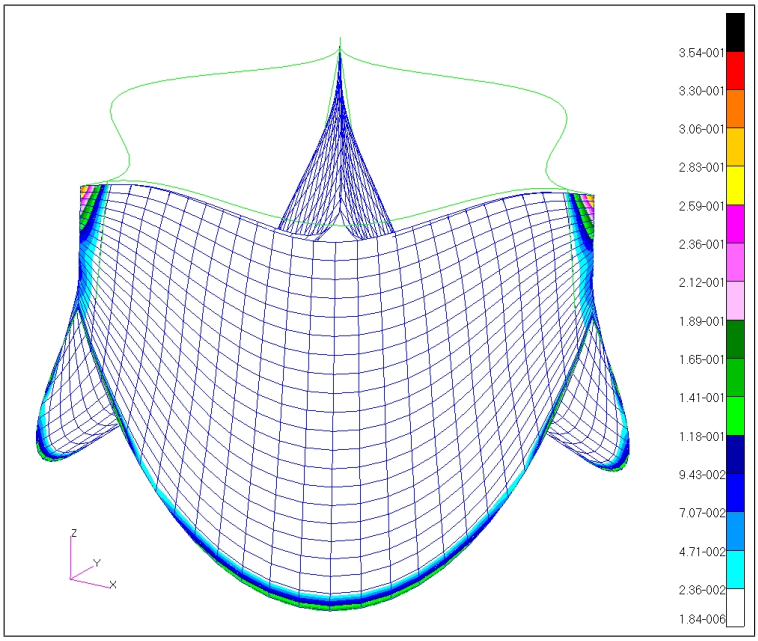

Figure 5.19: Valve Leaflet Force Distribution [5]

5.8.2 Simulation of Fatigue Loading

For the fatigue loading simulations, the discrete deformation modes, as described in Section 5.6, was first modeled to induce the steady state stresses in the models. The discrete deformation modes were followed by the fatigue load step. Since the deployed stent will be located on the aortic side of the valve leaflets, a dynamic pressure according to Figure 5.17 was applied to the internal surface of the stent to simulate the physiologic pressure cycle. For the leaflet reaction forces the results of the analysis by A. Smuts was used to formulate the force distribution across the stent. Therefore, along with the physiologic pressure cycle, a time-dependent force according to Figure 5.18 was distributed according to Figure 5.19 along the nodes on the models that corresponded to the assembly line between the stents and the valve leaflets.

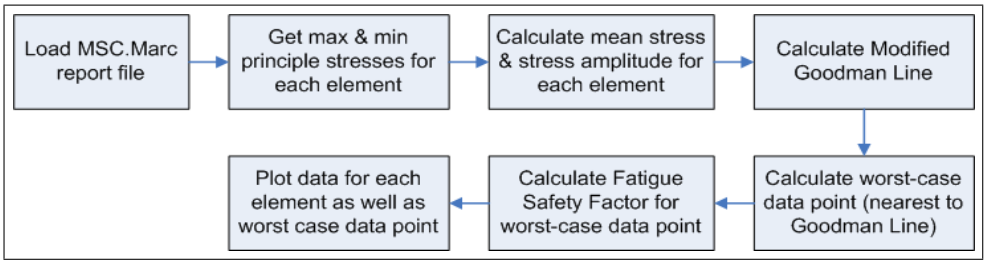

Figure 5.20: Diagram of MATLAB Script: Calculation of Fatigue Safety Factor

5.8.3 Fatigue Loading: Analysis of Results

According to literature the endurance limit (S_e) of stainless steel 316L is 260 MPa [37]. For the cyclic loading, as discussed in Section 5.8.2, the mean stress (σ_m) and stress amplitude (σ_a) were calculated for each element across the stent. The mean stress and stress amplitude were calculated from the predicted maximum principle stresses according to Equations 5.8.1 and 5.8.2 [36].

$$\sigma_m = \frac{\sigma_{max} + \sigma_{min}}{2} \tag{5.8.1}$$

$$\sigma_a = \left| \frac{\sigma_{max} - \sigma_{min}}{2} \right| \tag{5.8.2}$$

A MATLAB script was written to process the generated finite element data and calculate the fatigue life parameters for each of the strut widths. The code for the MATLAB script can be found in Appendix E. A diagram which shows the program flow of the MATLAB script is shown in Figure 5.20.

The calculated mean stress and stress amplitude for each element across the stent are shown as the blue dots in Figure 5.21 for Concept A (strut width = 0.23 mm) and Figure 5.22 for Concept B (strut width = 0.25 mm). In order to maintain the flow of the text, results of the MATLAB analyses for the remaining strut widths can be found in Appendix F.

The predicted mean stresses and stress amplitudes were used to calculate a Fatigue Safety Factor (FSF) distribution by utilizing the Modified

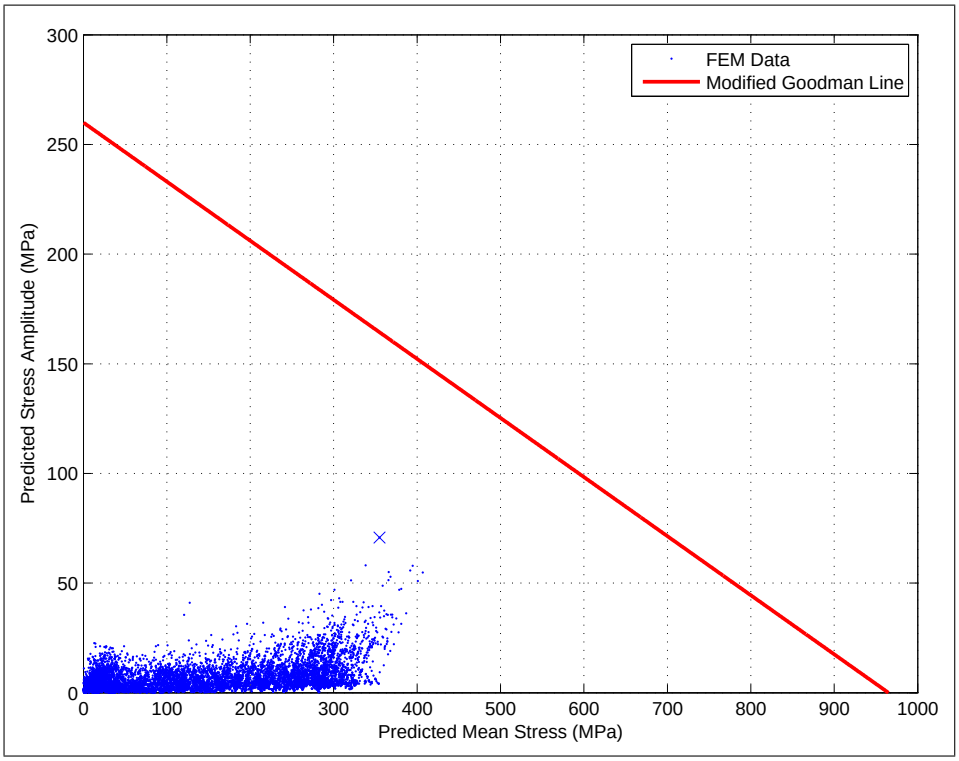

Figure 5.21: Concept A: Fatigue Diagram - Strut Width 0.23 mm

Goodman Failure Criteria. The FSFs give an indication of the proximity of the mean stress and stress amplitude at each numerical integration point to the Modified Goodman Line, which is also indicated in Figures 5.21 and 5.22. The "×" in each figure shows the data point which lies nearest to the Goodman Line and represents the element most susceptible to fatigue failure. The equation that defines the FSF for each numerical integration point is given in Equation 5.8.3, with S_{ut} being the ultimate true tensile strength [35].

$$\frac{\sigma_a}{S_e} + \frac{\sigma_m}{S_{ut}} = \frac{1}{FSF} \tag{5.8.3}$$

For both concepts the worst case FSFs, as represented by the "×" in the figures, are given in Tables 5.11 and 5.12.

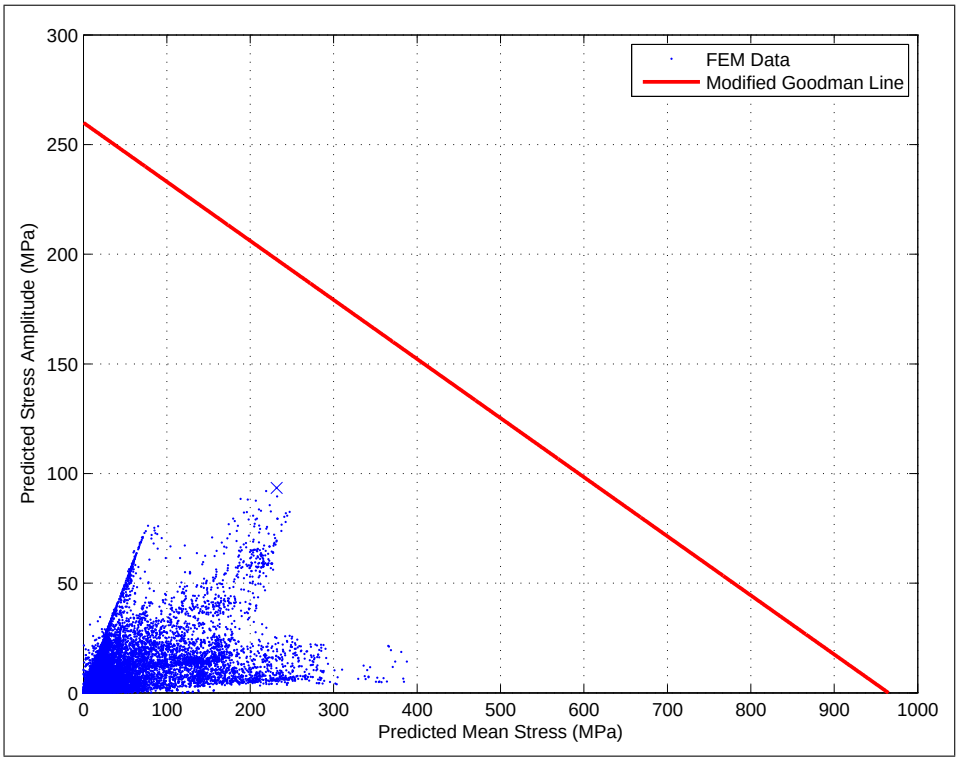

Figure 5.22: Concept B: Fatigue Diagram - Strut Width 0.25 mm

Table 5.11: FSF: Concept A

Strut Width (mm)	Mean Stress σ_m (MPa)	Stress Amplitude σ_a (MPa)	Fatigue Safety Factor (FSF)
0.20	462.91	55.15	1.45
0.23	354.99	70.74	1.56
0.25	487.07	31.93	1.59
0.27	497.44	23.67	1.65

Table 5.12: FSF: Concept B

Strut Width (mm)	Mean Stress σ_m (MPa)	Stress Amplitude σ_a (MPa)	Fatigue Safety Factor (FSF)
0.20	300.66	104.56	1.40
0.22	283.14	86.65	1.59
0.25	231.68	93.48	1.67
0.27	219.74	93.46	1.70

Table 5.13: Sensitivity Analysis

Parameter	FSF	# of iterations	Analysis Time (hours)
Default Parameters	1.67	82	5.22
Modified Newton-Raphson	1.68	218	9.99
Large Strain Multiplicative	1.69	99	4.41
Direct Profile	1.67	82	12.21

FSF = Fatigue Safety Factor

From the tables it can be seen that, for both concepts, an increase in strut width represents an increase in resistance to fatigue. The impact of the results reported in this section, is discussed in the Section 5.10.

5.9 Sensitivity Analysis

A sensitivity analysis was conducted to determine the stability of the simulation results with respect to the selected solution parameters. The sensitivity of the simulation results were investigated with respect to the following parameter changes:

- The iteration method was changed from the Newton-Raphson method to the Modified Newton-Raphson method
- The plasticity procedure was changed from Large Strain Additive to Large Strain Multiplicative
- The solver was changed from Multifrontal Sparse to Direct Profile

The results of the sensitivity analysis for the fatigue simulation of Concept B (strut width of 0.25 mm) is given in Table 5.13.

The results of the sensitivity analysis confirmed the stability of the simulation setup. It can be seen that the simulations were not particularly sensitive to a variation of the analysis parameters. The Direct Profile solver yielded exactly the same results as the Multiplicative Sparse

solver, however the analysis time was much slower. Selection of the Large Strain Multiplicative procedure resulted in a decrease of the analysis time while the FSF only changed marginally.

5.10 Discussion of Numerical Results

5.10.1 Concept A vs. Concept B

It can be seen from the geometric parameters of the stent concepts (Section 5.1) that Concept A exhibits a lower metal-to-surface area ratio compared to Concept B. It can also be seen that Concept A has a shorter deployed length. The geometric parameters indicate that Concept A has a lower profile when compared to Concept B. This is advantageous as it is desirable for the valve device to have the lowest profile possible. Note that the overall undeformed length and deployed length for Concept B is the same. This may be attributed to the fact that the three support struts do not experience a change in length during the various deformation modes.

For Concept A, a considerably higher pressure was required to deploy the stent to the functional diameter (Section 5.7.2). A higher deployment pressure implies a higher radial strength. A high radial strength is advantageous as it provides an increased resistance to radial compressive forces. A high deployment pressure, however, has the disadvantage that deployment by manual pressurisation becomes more difficult and risk factors such as uneven deployment as well as balloon rupture comes into play.

Concept A exhibits a slightly smaller crimp diameter as compared to Concept B (Section 5.7.3). Crimp diameter plays a major role in the performance of the valve device as it determines the ease with which the device may be guided through the arterial pathways. In this regard, Concept A is superior to Concept B.

An analysis of the accumulated stresses and strains indicated that, for the same strut widths, both concepts exhibited similar safety factors

against failure (Section 5.7.4). As the problem at hand was regarded as an induced strain problem as opposed to an induced stress problem, attention was given to the safety factors against strain failure. Since Concept B exhibited slightly larger safety factors against strain failure for comparable strut widths, Concept B presented a superior concept is this respect.

An analysis of the mode of deformation (Section 5.7.5.1) indicated that Concept A and Concept B exhibited entirely different deployment deformations. As mentioned, Concept A exhibited a "dog-boning" deformation mode, while Concept B exhibited a "coning" deformation mode. Although the actual impact of these deformation modes on the ease and effectiveness of in-vivo deployment was difficult to predict, it is evident that a "dog-boning" deformation mode might result in a self-positioning phenomenon, which would be advantageous. No inherent advantages could be foreseen regarding the "coning" deformation mode.

The analysis of the elastic recoil (Section 5.7.5.2) indicated that the longitudinal recoil for both concepts were less than 1%, which would have a negligible impact on the performance of the stents. Radial recoil is an important parameter with respect to stent performance. It is desirable for a stent to exhibit a minimal radial recoil, because radial recoil will counteract the anchoring of the device within the aortic annulus. For similar strut widths, Concept A showed slightly less radial recoil as compared to Concept B.

It is predicted that foreshortening of the stent will play a significant role in the performance of the valve device as it will influence the amount of strain transferred from the sutures to the valve leaflets during the deployment process. Since the sutures will be displaced along with the struts of the stent during the deployment step, a significant amount of foreshortening might lead to high stresses and unnatural deformations induced in the leaflets. An analysis of the foreshortening induced in both concepts (Section 5.7.5.3) indicated that Concept A would experience approximately twice the percentage of foreshortening compared to concept B. With respect to foreshortening, the analysis indicated that Concept B showed superior performance compared to Concept A.

An analysis of the resistance to fatigue failure (Section 5.8) indicated that for similar strut widths, both concepts exhibited very similar resistances to fatigue failure. Since a worst-case fatigue loading scenario was investigated with physiologic conditions that is very unlikely to occur in an actual situation, a fatigue safety factor in the range of 1.4-1.7 was deemed sufficient. Since both concepts exhibited similar resistances to fatigue, neither concepts appeared to be superior in this regard.

A summary of the most significant results from the numerical analyses is given in the following list:

- Concept A exhibits a comparatively lower metal-surface area ratio. Metal-surface area ratio is directly related to the amount of metal placed inside the patient per surface area. It is desirable to have a minimum metal-surface area ratio as to reduce the bulkiness of the device as well as to improve the bio-compatibility of the device.
- Concept A has a shorter deployed length. A short deployed length is advantageous as it reduces possible interference with the coronary arteries.
- Concept A has a smaller crimp diameter and lower profile.
- Concept A exhibits a comparatively higher radial strength.
- Concept B exhibits a comparatively higher safety factor against strain failure.
- Concept A conforms to a dog-boning deloyment mode, whereas Concept B conforms to a coning deployment mode.
- Concept A shows comparatively less radial recoil.
- Concept B shows comparatively less foreshortening.

5.10.2 Selection of Strut Width

With respect to the selection of a strut width for the final design, for some of the parameters discussed in the preceding sections, a thinner strut width is preferred, while for others a thicker strut width is advantageous. Therefore, when selecting a strut width, a compromise much be reached between the parameters. Therefore a careful consideration of the importance of each parameter is required with respect to each of the concepts.

5.10.2.1 Concept A

Since Concept A presents an inherently larger radial strength, a smaller strut width is desirable to achieve a realistic deployment pressure. This will also be a benefit for the minimum crimp diameter and strains induced within the stent. The FEM analyses indicated that the amount of dogboning increases slightly with an increase in strut width. As discussed, with respect to the stent application a fair amount of "dogboning" is desirable, however too much dogboning might also result in poor performance. With respect to Concept A, the strut width has a limited effect on both the amount of radial recoil and foreshortening. A larger strut width will be beneficial to the resistance against fatigue failure. In order to obtain a reasonable deployment pressure and minimise the crimp diameter and induced strains, while achieving a reasonable amount of dogboning and an FSF of at least 1.56, a strut width of 0.23 mm was selected for the final design.

5.10.2.2 Concept B

Since Concept B exhibits an inherently smaller radial strength, a larger strut width would be required to achieve a deployment pressure and radial strength comparable with Concept A. As is the case with Concept A, a smaller strut width will allow for a smaller achievable crimp diameter as well as smaller induced strains. The analyses indicated that the amount of "coning" was not dependent on the strut width. With re-

spect to Concept B, the amount of radial recoil as well as foreshortening decreases slightly with an increase in strut width. A larger strut width will also be beneficial to the resistance against fatigue failure. In order to achieve an improved radial strength, while maintaining a reasonable crimp diameter, a slightly larger strut width was selected compared to Concept A. A strut width of 0.25 mm was selected for Concept B, since the larger strut width also resulted in less radial recoil and foreshortening, which was desirable. The selected strut width gave a safety factor against fatigue of 1.67, being slightly larger as compared to Concept A.

Chapter 6

Manufacturing and Electropolishing

6.1 Manufacturing of Stent Prototypes

Stent manufacturing is a highly specialised field, which involves high costs and requires advanced manufacturing equipment. As a result, for the first protoype development phase, only 10 prototype stents were manufactured for each of the two final designs selected in Section 5.10.2. The stent prototypes were laser cut courtesy of Disa Vascular (Pty) Ltd, a leading South African stent manufacturing company. Figures 6.1 and 6.2 show photos of the two designs that were selected for prototype manufacturing.

6.2 Electropolishing

6.2.1 Introduction

The manufacturing of stents by the laser cutting process results in the stents having sharp edges. It is therefore common practise in the stent manufacturing industry to electropolish stents following the cutting process. This is done to remove sharp edges and surface irregularities, to

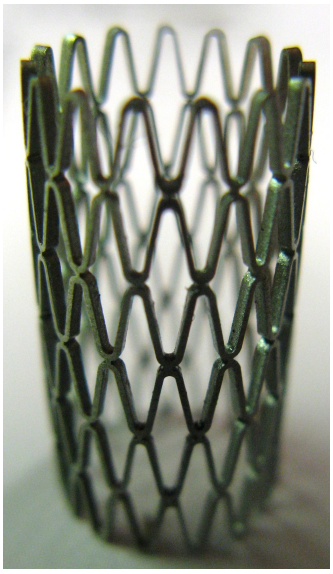

Figure 6.1: Concept A: Prototype Stent

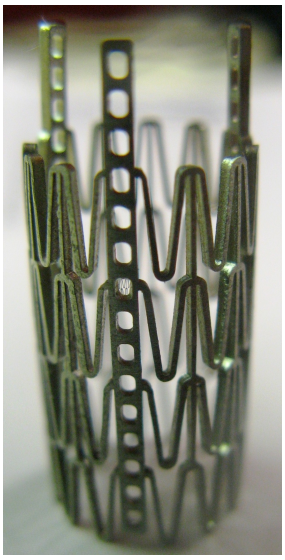

Figure 6.2: Concept B: Prototype Stent

control surface levelling and to improve surface smoothness. The process may be controlled by varying the following parameters [38]:

- Voltage potential and applied current
- Electrolite composition and concentration
- Electrolite temperature
- Processing time
- Hydrodynamics (agitation, cell configuration and geometry)
- The untreated surface quality

6.2.2 Electropolishing Parameter Setup

According to a representative of Disa Vascular (Pty) Ltd, the company's research indicated that the following electrolite composition (by weight) works well to electropolish stents manufactured from stainless steel 316L [39]:

- 40 parts: 85% Phosphoric acid
- 39 parts: 99% Glycerol
- 11 parts: Deionised water

The representative also recommended the following processing parameters as a starting point:

- Voltage potential: 15 V
- Electrolite temperature: 70 °C
- Processing time: 1-2 minutes, depending on the amount of stock removal required

Since Disa Vascular has about 10 years of experience regarding stent manufacturing and electropolishing, it was decided that their parameter recommendation would be used as a starting point for the electropolishing process.

6.2.3 Electropolishing Process Setup

Figure 6.3 shows a diagram of the setup that was used to conduct the electropolishing process.

The heated magnetic stirrer plate contains a rotating magnet which agitates the stirrer magnet placed inside the glass beaker. The electrolite temperature and agitation could therefore be controlled by the stirrer plate. A piece of thin 316L sheet metal was rolled up to form a roughly tubular structure and placed inside the beaker to act as the cathode. The stent, which acted as the anode, was suspended from a Tungsten wire into the center of the immersed cathode tube to ensure that it saw an equal electric field. The cathode tube was connected to the negative terminal and the stent to the positive terminal of a 20 V 5 A DC power supply.

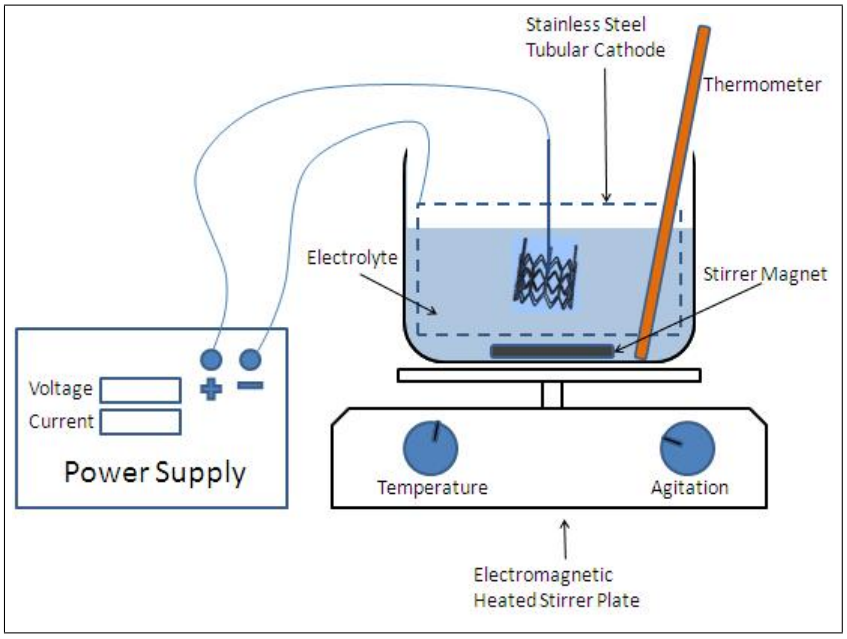

Figure 6.3: Electropolishing Process Setup

6.2.4 Electropolishing Results

Figure 6.4 shows a magnified image of a section of one of the untreated prototype stents. From the figure it can be seen that the untreated stent had a fairly poor surface finish and that the surface contained irregularities and impurities. This could be attributed to the fact that non-medical tubing was used to manufacture the stents. It was expected that, as a result of the poor untreated surface finish, the advantageous outcome of the electropolishing process would be limited.

Since the geometries of the stent designs were set, the outcome of the electropolishing process would be determined by the electrolite temperature, voltage potential, agitation and processing time. Since these four parameters could yield an endless number of possible combinations, it was decided that the agitation and voltage potential would be set, while the temperature and processing time would be varied in an attempt to achieve satisfactory electropolishing results. A number of tubing off-cut samples were used to experiment with the variable parameters. The results of these experiments are presented in Appendix D. The results of

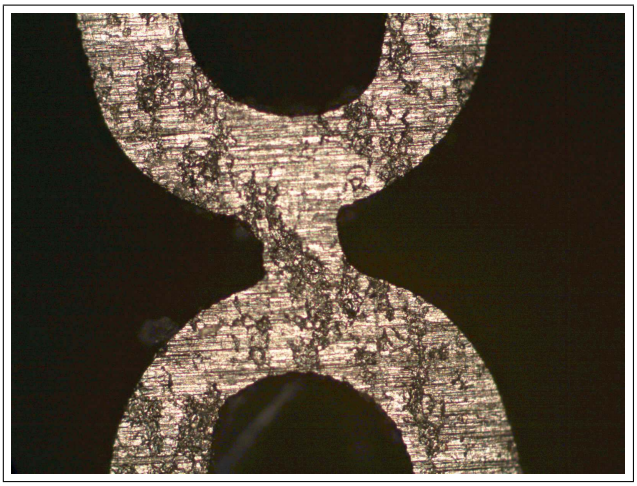

Figure 6.4: Untreated Stent - 100x Magnification

these samples indicated that pitting (formation of crevices) of the surface started immediately at the onset of the electropolishing process and was unavoidable. It appeared that this may be attributed to the poor untreated surface finish. It also appeared as though a variation in temperature had a greater influence on the results as compared to a variation in processing time. The results of the samples were used as a basis to investigate the parameters that would give the best possible surface finishes for the prototype stents. The aim was to brighten the surface and smoothen the edges without compromising the stent structure. The parameters that worked best for the stent prototypes are given in Table 6.1. Figures 6.5 and 6.6 show magnified sections of stent prototypes that were electropolished with these parameters.

Although the results obtained are far from optimal, the electropolishing process aided in smoothing the sharp stent edges, which would otherwise present a possible threat to balloon rupture as well as suture and leaflet damage. It can also be seen from the results that the processing time for Concept A is considerably higher compared to the processing time for Concept B. This could be attributed to the difference in stent geometry.

Table 6.1: Stent Prototype Electropolishing Parameters

	Voltage (V)	Agitation	Temperature (°C)	Processing Time (s)
Concept A	16	3/6	85	240
Concept B	16	3/6	78	135

Figure 6.5: Microphotograph of Concept A Prototype: Polished Surface

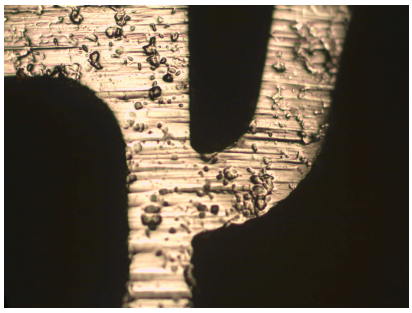

Figure 6.6: Microphotograph of Concept B Prototype: Polished Surface

6.3 Assembly of Valve Prototypes

Although the assembly of the valve prototypes did not form a part of this thesis, a photo of each of the assembled concepts is included in this section to confirm the compatibility of the concepts with the respective assembly configurations. The valve prototypes were assembled by Mr. A. Smuts as part of his Master's thesis. Figure 6.7 shows one of the prototypes that were assembled according to Concept A and Figure 6.8 shows one of the prototypes that were assembled according to Concept B.

Figure 6.7: Concept A - Assembled Prototype

Figure 6.8: Concept B - Assembled Prototype

Chapter 7

Experimental Analysis

In order to perform an initial evaluation of the performance and characteristics of the manufactured prototype stents, the discrete deformation and loading modes to which the stents will be subjected during assembly and deployment (Section 5.6) were experimentally replicated in an in-vitro environment. The experimental results also served to evaluate the reliability of the finite element simulations.

7.1 Experimental Procedure

The simulated deformation and loading modes were experimentally replicated by performing the steps described in this section. For each of the steps, the distal, proximal and central outer diameters as well as the lengths of the stents were measured at regular intervals by means of a digital vernier caliper.

7.1.1 Rigid Expansion Process

The initial rigid expansion of the stents was achieved by advancing the stents across a stainless steel polished tapered rod, which was specifically manufactured for this purpose. The diameter of the tapered rod increased from 8 mm to 20.2 mm at a taper angle of 1.06 degrees. The stents were slightly over expanded to compensate for elastic radial re-

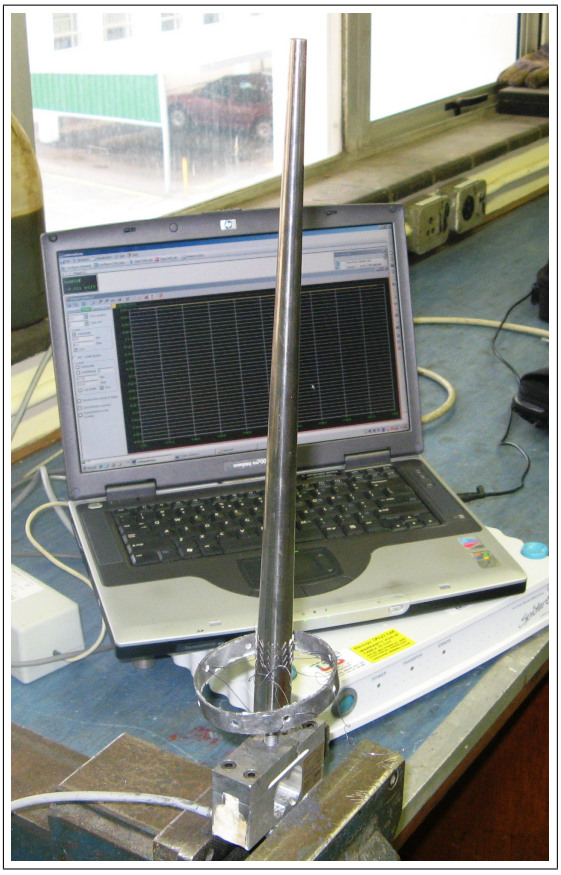

Figure 7.1: Photo of Taper Expansion Setup

coil. To achieve this process, the stents were first attached to a PVC ring with strong sutures. The PVC ring was subsequently advanced over the tapered rod to achieve an even expansion of the stents. Graphite powder was used as a lubricant. Figure 7.1 shows a photo of the setup that was used for the rigid expansion process. Figure 7.6 (Section 7.2.2) shows a diagram of the rigid expansion process.

7.1.2 Crimping Process

The crimping process was achieved by crimping the stents onto a balloon catheter by hand. The first phase of the hand crimping was achieved by crimping the stents against the tapered stainless steel rod, which served as a crimping guide. The final phase of the hand crimping was achieved

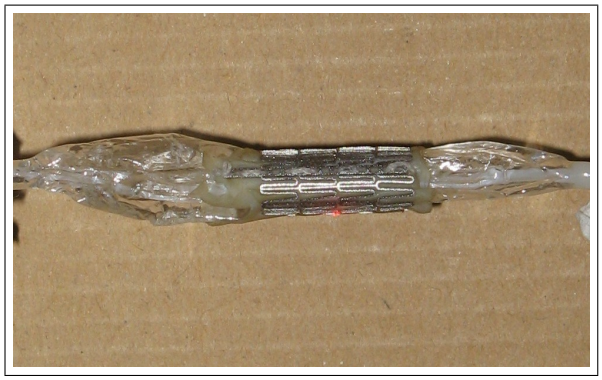

Figure 7.2: Concept B Prototype: Crimped State

by crimping the stents, over a thin pericardium sheath, onto the balloon catheter. The sheath served to represent the valve leaflets as well as protect the balloon from rupture. Figure 7.2 shows the crimped state for one of the prototypes of Concept B.

7.1.3 Deployment Process

As described in Section 7.1.2, the prototype stents were crimped onto a low-compliance NuMed^{TM} PET (polyester polyethylene terephthalate) balloon catheter with a rated deployment diameter of 18 mm and a burst pressure of 6 bar. Prior to the deployment step, the balloon catheter was filled with saline and flushed to remove any trapped air bubbles. Subsequently, the stents were gradually deployed to the deployment diameter by increasing the pressure through a syringe, which was connected to the corresponding catheter port. The deployment pressure was monitored using a pressure gage, connected to a side port. Figure 7.3 shows a photo taken during the deployment process for a prototype stent of Concept A.

7.1.4 Elastic Recoil

After the deployment process, the internal balloon pressure was removed to allow for the elastic recoil of the stents.

Figure 7.3: Concept A Prototype: Deployment Process

7.1.5 Fatigue Loading

In order to evaluate the resistance of the stents to the fatigue loads, as would be typically experienced by the stents in an in-vivo environment, it was initially proposed that the assembled valves be subjected to accelerated fatigue tests in a pulse duplicator. A pulse duplicator is a machine which simulates the pumping action of the left ventricle. The design and construction of a pulse duplicator formed part of another Master's thesis. Unfortunately, at this point in time, the pulse duplicator still experiences some technical difficulties during operation which prevents it from operating for extended periods of time. Therefore, fatigue tests could not yet be conducted and the fatigue simulations could not be validated.

7.2 Discussion of Experimental Results

7.2.1 Stent Deployment Process

Figures 7.4 and 7.5 show, for both concepts, plots of the distal outer diameters vs. deployment pressures for the experimental data as well as the simulation results. From the plots it can be seen that, for both concepts, the simulated deployment pressure is considerably higher compared to the actual required deployment pressure. It seems probable that this may be attributed to the effect of the outward vectored forces of the bulging balloon membrane, in between the struts, that is not taken into account in the finite element simulations [40]. During the actual deployment of

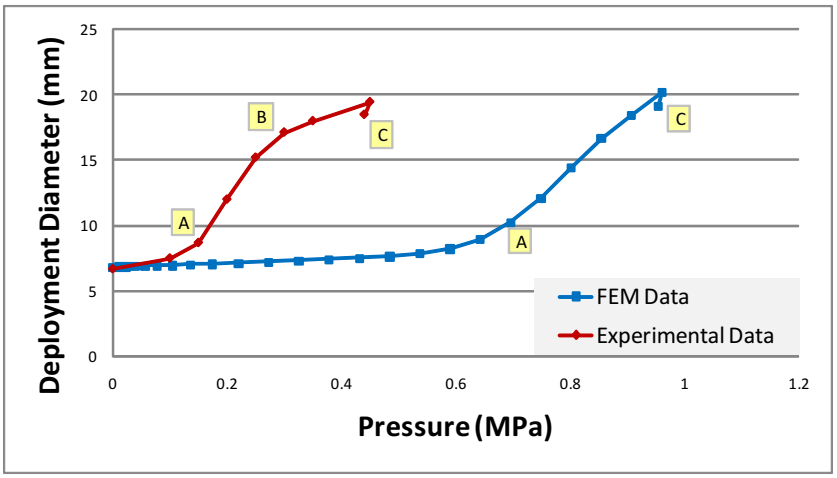

Figure 7.4: Concept A Prototype: Deployment Pressure vs. Displacement - Comparison of Results

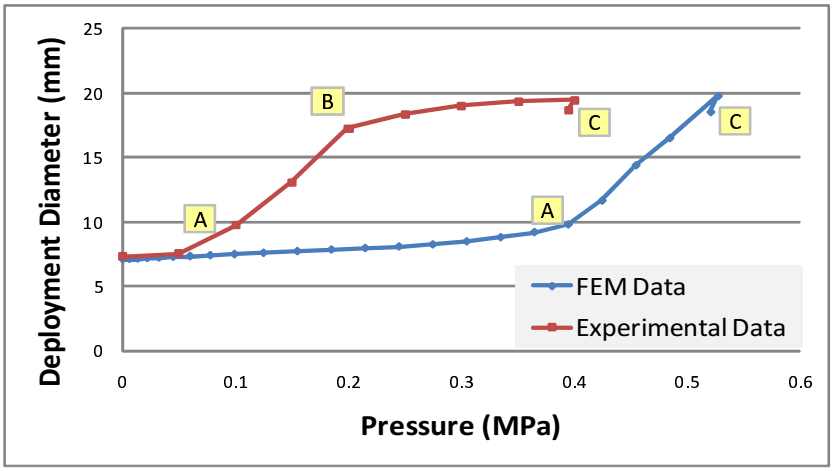

Figure 7.5: Concept B Prototype: Deployment Pressure vs. Displacement - Comparison of Results

the stent a load of unknown magnitude is transferred by the membrane to the stent as the balloon expands. The results could therefore not be used to verify the validity of the simulations.

The results could however be used to indicate the actual pressure required to deploy the stents. The experimental results confirmed that Concept A required a larger deployment pressure, as suggested by the finite element simulations. The deployment pressure for Concept A was

0.25 MPa, while the deployment pressure for concept B was 0.2 MPa. The deployment pressure was taken as the point at which the required deployment pressure was no longer dominated only by the resistance from the stents, but also by the resistance of the balloon, as it neared its nominal deployment pressure (Symbol "B" in the figures).

It should also be noted that there existed a correlation between the simulation data and experimental data for the diameters at which the stents experienced a transition from the elastic deployment deformation to plastic deployment deformation, indicated by symbol "A" in the figures.

For both the simulation and experimental data, symbol "C" indicates the amount of elastic radial recoil which takes place when the deployment pressure is removed.

7.2.2 Rigid Expansion Process

As a result of the fact that the experimental results of the deployment process failed to validate the finite element simulations, an experiment had to be designed to verify the validity of the simulations. For this purpose an experimental setup was constructed to measure the reaction force applied to the tapered expansion rod as the stents were expanded by advancing them across the rod.

For this experimental setup, the tapered rod was mounted to a 500 N load cell and the force required to advance the stents across the rod was recorded, using a SPIDER^{TM} bridge amplifier / data acquisition system, against the instantaneous translated distance along the rod. Although only a small part of the load cell range was used, a calibration test was conducted which indicated that the load cell was linear and accurate in this range. Graphite powder was used as a lubricant. Figure 7.6 shows a diagram of the experimental setup that was used.

For both stent concepts, this process was also subjected to a finite element analysis. Since the coefficient of friction between the stents and the taper was an unknown variable, the simulations for both concepts were

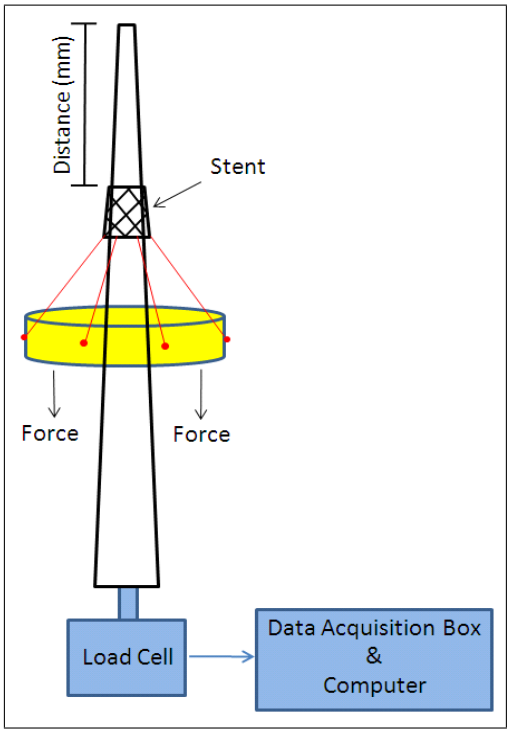

Figure 7.6: Diagram of Taper Expansion Process

conducted for different friction coefficients.

The experimental results as well as the results of the finite element simulations for different coefficients of friction are given for Concept A in Figure 7.7 and for Concept B in Figure 7.8. From these results it can be seen that for Concept A, a coefficient of friction of 0.085 correlated well with the experimental results, while for Concept B a coefficient of friction of 0.1 correlated well with the experimental results. These results indicated that the geometric models, mesh densities and material properties used to describe the FEM models could, to a certain extent, be implemented in finite element analyses to predict the behavior of the concepts.

7.2.3 Modes of Deployment

For Concept A, the "dog-boning" effect (Equation 5.7.1) is plotted as a function of central outer diameter in Figure 7.9 for both the experimental

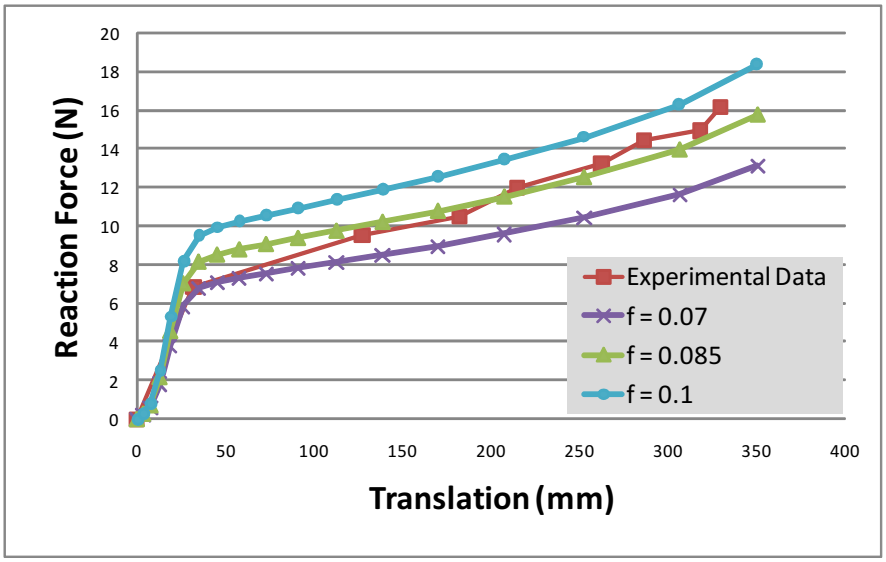

Figure 7.7: Concept A: Rigid Expansion - Comparison of Results

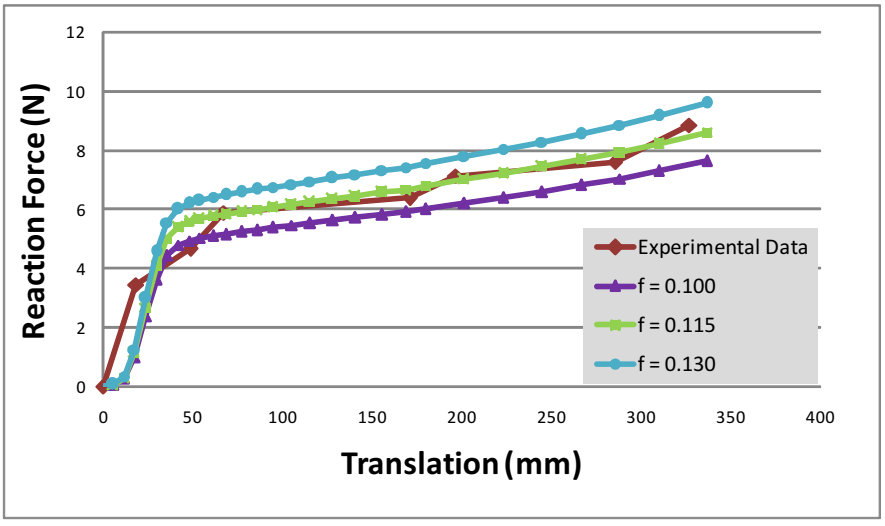

Figure 7.8: Concept B: Rigid Expansion - Comparison of Results

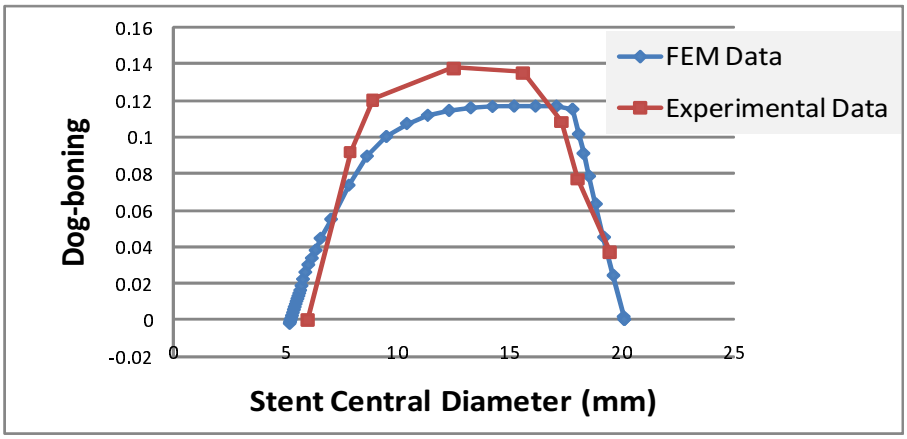

Figure 7.9: Concept A: Dog-boning - Comparison of Results

results as well as simulated results. From the figure it can be seen that the maximum dog-boning for the experimental results is somewhat higher compared to the simulation data. It is again plausible that the effect of the balloon membrane played a role in the deviation of the experimental results from the simulation data. Other factors such as non-uniform strut width may also have attributed to the discrepancy between the data sets.

For Concept B, the coning effect (Equation 5.7.2) is plotted as a function of the stent outer diameter in Figure 7.10 for both the experimental results as well as the simulated results. From the figure it can be seen that the maximum coning for the experimental results is slightly higher compared to the simulation data. Apart from the discrepancy between the maximum coning, the experimental data correlates well with the simulation data.

7.2.4 Crimp Diameter, Foreshortening and Recoil

The parameters for minimum crimp diameter, foreshortening and elastic recoil were also compared for the simulation data and experimental data. The results for the comparison is given in Table 7.1. The deviation of the simulation data from the experimental results is also given as a percentage in the table. From the comparison of the simulation data and experimental data it can be seen that the simulations predicted the min-

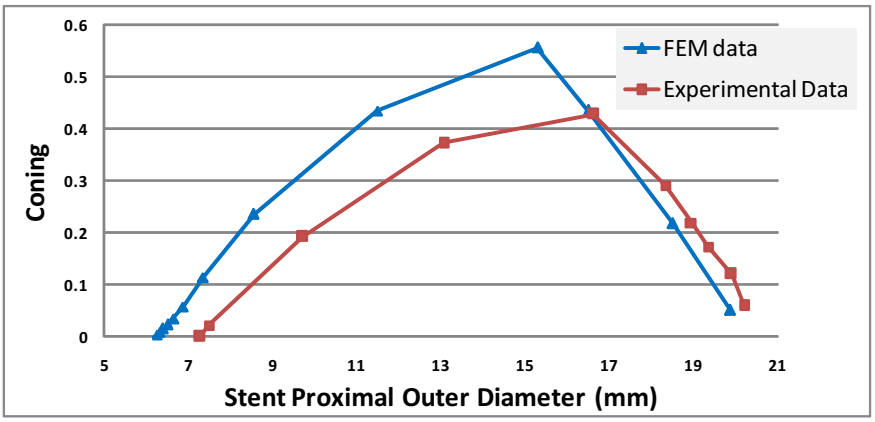

Figure 7.10: Concept B: Coning - Comparison of Results

Table 7.1: Parameter Comparison: Experimental Data vs. Simulation Data

Concept A	Simulation Results	Experimental Results	Deviation (%)
Min. Crimp Dia. (mm)	4.64	4.71	1.5
Foreshortening (%)	8.67	10.12	14.3
Radial Recoil (%)	5.53	5.20	6.3
Longitudinal Recoil (%)	-0.86	-0.92	6.5

Concept B	Simulation Results	Experimental Results	Deviation (%)
Min. Crimp Dia. (mm)	5.43	5.27	3.0
Foreshortening (%)	4.00	3.54	13.0
Radial Recoil (%)	6.30	6.03	4.5
Longitudinal Recoil (%)	-0.55	-0.49	12.2

imum crimping diameter to an accurate degree. For both concepts the parameter for foreshortening was predicted to the least accurate degree. This was unexpected as foreshortening is a geometry dependent parameter as opposed to a material dependent parameter and a higher accuracy would be expected. The parameters for recoil were predicted within an 13% margin, which, from an engineering point of view, is a reasonable deviation.

7.3 Conclusion to the Experimental Analysis

Although there were some discrepencies between the data obtained from the simulations and the experimental results, the experimental analysis served to provide a good insight into the actual performance characteristics of the concepts as well as to provide insight into the value of finite element simulations with respect to stent design and development.

From the experimental analysis, the actual required deployment pressure was determined, the mode of deployment for each concept was evaluated and other stent characteristic were measured. The knowledge gained from the experimental analysis will be invaluable for continued prototype development and refinement.

Chapter 8

Conclusion

The literature review indicated that the development of a percutaneous aortic heart valve is an intricate process which is extremely time consuming and costly. It is therefore imperative that modern technologies be implemented to reduce the number of design iterations required to develop a functional device. Since the finite element method provides an cost and time effective tool to perform structural analyses, it was the objective of this thesis to implement this technology to develop, taking into account time and cost efficiency, a first prototype for the stent component of a percutaneous aortic heart valve, which would serve as the stepping stone towards continued product development.

In order to achieve this objective a number of stent concepts were generated. The two most promising concepts were subjected to comprehensive finite element analyses of the deformations and forces experienced by the stent during implantation and operation. For each of the most promising concepts, the simulations were conducted for different strut widths to determine the strut width that would be most suited for the specific stent application. The results of the FEM simulations indicated that a variation in strut width had a substantial influence on stent characteristics such as radial strength, crimp diameter, stress and strain, elastic recoil and fatigue. Stent characteristics such as mode of deformation and foreshortening were less influenced by strut width. The results also indi-

cated that the selection of stent geometry had a major influence on stent performance.

From the results of the FEM analyses a strut width was selected for each concept and a number of prototypes were manufactured. The prototypes were subjected to experimental analyses to evaluate the relevance of the FEM analyses as well as to evaluate the actual stent performance. Although the FEM analyses were able to predict some of the stent characteristic to a fairly accurate degree, the overall performance of the stents were compromised by non-uniform strut width and poor surface finishes. The use of non-medical grade tubing resulted in non-uniform strut widths due to the fact that the laser beam had trouble maintaining a pinpoint focus on the tubing which had a low concentric tolerance. An important conclusion that may be drawn from this result is that the use of high grade medical tubing is vital for optimal stent performance.

The most significant conclusion that could be drawn from the finite element simulations and experimental work was that Concept A is the most promising stent design. For comparable strut widths, Concept A showed a lower metal-surface area ratio, a higher radial strength, a smaller crimp diameter and slightly less radial recoil. Concept A was compatibile with the parabolic leaflet assembly configuration, which is the configuration which most accurately resembles the native aortic valve. Concept A also exhibited a dog-boning deployment mode, which might be beneficial to the positioning of the device. A single drawback of Concept A was that it exhibited a greater amount of foreshortening compared to Concept B. However, testing of the prototype valves assembled by Mr. A. Smuts indicated that this was not a significant drawback.

An additional conclusion that can be drawn is that the electropolishing process failed to achieve a significant improvement of the fairly poor surface quality of the metal tubing used. As a result of this, the optimal electropolishing parameters for the specific stent geometries could not be determined.

Through the research conducted, the author gained experience in the simulation of non-linear finite element problems. A better understanding

was also achieved regarding the aspects involved in the development of a percutaneous aortic heart valve and knowledge was gained regarding the design parameters that determine stent performance characteristics.

As a step towards developing a functional product, an application for a provisional patent has been submitted for a percutaneous aortic heart valve which utilises Concept A.

Chapter 9

Limitations and Recommendations

The work done in this Master's thesis served as a stepping stone towards the development of a percutaneous aortic heart valve that will eventually be suitable for implantation in human beings. It is therefore vital that the knowledge gained through the research conducted be transferred to the entity that will continue the research and development of the device. The goal of this section is therefore to highlight the limitations of the current work as well as provide recommendations for future research on the subject.

9.1 Limitations to the Work

The following limitations to the current work were identified:

- The external environment, such as the radial reaction force exerted by the aortic annulus, was not considered for finite element simulations.
- The effect of the bulging balloon-membrane on the deployment of the stents was not considered for the finite element simulations.

- The simulations and experimental work was conducted for stainless steel instead of the more superior cobalt-chrome alloy, MP35N of L605.
- The effect of a variation in strut thickness was not considered.
- Fatigue performance of the prototypes were not evaluated in a pulse duplicator.

9.2 Recommendations

Based on the results and limitations to the work, the following recommendations can be made for continued development of a fully functional percutaneous aortic valve replacement:

- Since the results of the present work indicated that Concept A is the most promising concept, it is recommended that continued development of the prototype be focused on this concept.
- Medical grade cobalt-chrome (MP35N) tubing must be used instead of lower grade stainless steel to manufacture the prototypes.
- Since cobalt-chrome exhibits slightly superior properties compared to stainless steel, it is recommended that the design for Concept A be slightly altered prior to the next round of prototype manufacturing. It is recommended that the strut thickness and strut width be slightly reduced. Also, since the actual deployed length of the prototype stent was slightly less compared to the simulated deployed length, the overall length of the stent may be slightly increased. The suggested dimensions for the next round of prototype manufacturing is given in Figure G.1 of Appendix G. The main purpose of these alterations is to give a slight reduction in deployment stiffness, as the experimental results indicated that the present design is slightly too stiff.

- The optimal electrolyte composition and electro-polishing parameters must be determined for a prototype stent manufactured from cobalt-chrome.
- A suitable test-rig must be designed and constructed to improve the accuracy of the experimental results.
- A crimping tool must be developed that is capable of achieving the uniform crimping of the assembled prosthesis.
- A delivery system must be developed and manufactured that is compatible with the valve prosthesis being developed.
- In-vitro fatigue tests must be conducted for the assembled prototype valves.
- The animal trial phase must be initiated.

List of References

[1] Cleveland-Clinic: Catalyst news. vol 3, Issue 3. (Cited on pages xi and 3.)

[2] David Chua, S., MacDonald, B. and Hashmi, M.: Effects of varying slotted tube (stent) geometry on its expansion behavior using finite element method. *Journal of Materials Processing Technology*, vol. 155-156, pp. 1764–1771, 2004. (Cited on pages xi, 13, 14, and 15.)

[3] UK, P.: Cardiac catheterisation. 2008.
Available at: `http://www.patient.co.uk/showdoc/40000522/` (Cited on pages xi and 34.)

[4] van Aswegen et al., K.: *Dynamic Modelling of a Stented Aortic Valve*. Master's thesis, University of Stellenbosch, 2008. (Cited on pages xii, 4, 52, and 53.)

[5] Smuts, A.e.a.: *Investigation of tissue materials for implamentation in a Percutaneous Aortic Heart Valve*. Master's thesis, University of Stellenbosch, 2008. (Cited on pages xii, 4, 25, 52, and 54.)

[6] University of maryland medical center, valvular disease. 20/05/2008.
Available at: `http://www.umm.edu/heart/valve_diseases.htm` (Cited on pages 1 and 2.)

[7] Stanford hospital, valvular disease.
Available at: `http://www.stanfordhospital.com/clinicsmedservices/coe/heart/diseasesconditions/valvularheartdisease/default` (Cited on page 1.)

[8] Ye, J., Cheung, A., Lichtenstein, S., Pasupati, S., Carere, R., Thompson, C., Sinhal, A. and Webb, J.: Six-month outcome of transapical transcatheter

aortic valve replacement in the initial seven patients. *European Journal of Cardiothoracic Surgery*, vol. 31, p. 16, 2007. (Cited on page 2.)

[9] Cervantes, J.: Fiftieth anniversary of the first aortic valve prosthesis implantation. *Langenbecks Arch Surg*, vol. 388, p. 366367, 2003. (Cited on page 2.)

[10] Weich, H.: E-mail correspondecse with author, 15 october 2007. (Cited on pages 2 and 22.)

[11] Boudjemline, Y. and Bonhoeffer, P.: Steps toward percutaneous aortic valve replacement. *American Heart Association*, 2002. (Cited on pages 3 and 8.)

[12] Brodsky, A.M.: Percutaneous approaches to aortic valve replacement. *Cardiac Interventions*, December 2004. (Cited on pages 3 and 8.)

[13] Joudinaud, T.M. and Flecher, E.M.: Sutureless stented aortic valve implantation under direct vision. *J Card. Surg.*, vol. 22, pp. 13–17, 2007. (Cited on page 3.)

[14] Anderson, H., Knudsen, L. and Hasenkam, J.: Transluminal implantation of artificial heart valves. description of a new expandable aortic valve and initial results with implantation by catheter technique in closed-chest pigs. *European Heart Journal*, vol. 13, pp. 704–708, 1992. (Cited on page 8.)

[15] Lutter, G.e.a.: Percutaneous aortic valve replacement: An experimental study. i. studies on implantation. *Journal of Thoracic and Cardiovascular Surgery*, vol. 123, pp. 768–776, 2002. (Cited on page 8.)

[16] Boudjemline, Y. and Bonhoeffer, P.: Percutaneous implantation of a valve in the descending aorta in lambs. *European Heart Journal*, vol. 23, pp. 1045–1049, 2002. (Cited on page 8.)

[17] Cribier, A., Eltchaninoff, H. and Bash, A.: Percutaneous transcatheter implantation of an aortic valve prosthesis for calcific aortic stenosis. *Circulation*, vol. 106, pp. 3006–3008, 2002. (Cited on page 8.)

[18] Gilad, R. and Somogyi, R.: Percutaneous heart valves: The emergence of a disruptive technology. *University of Toronto Medical Journal*, vol. 82, pp. 200–201, 2005. (Cited on page 9.)

[19] CoreValve: Corevalve: The revalving technology. 2008.
Available at: `http://www.corevalve.com` (Cited on page 9.)

[20] Poncin, P. and Proft, J.: Stent tubing: Understanding the desired attributes. In: *Materials & Processes for Medical Devices Conference*. 2003. (Cited on pages 9, 10, 11, 21, 22, 23, and 44.)

[21] Meyer-Kobbe, C.: The importance of annealing 316 lvm stents. *Medical Device Technology*, pp. 19–21, January 2003. (Cited on page 11.)

[22] Amit Datye, K.H.: Effect of strut thickness, crimping and expansion diameters on radial strength, recoil and foreshortening of a coronary stent. Department of Mechanical and Materials Engineering, Florida International University. Miami. (Cited on pages 12, 13, 15, and 16.)

[23] Hibbeler, R.: *Mechanics of Materials. 2nd Edition*. Macmillan, 1994. (Cited on page 15.)

[24] Kastrati, A., Dirschinger, J. and Boekstegers, P.: Influence of stent design on 1-year outcome after coronary stent placement, a randomized comparison of five stent types in 1147 unselected patients. *Catheterization Cardiovascular Intervention*, vol. 50, pp. 290–297, 2000. (Cited on page 15.)

[25] Barth, K., Froelich, J. and Virmani, R.: Paired comparison of vascular wall reactions to palmaz stents, strecker tantalum stents, and wallstents in canine iliac and femoral arteries. *Circulation*, vol. 93, pp. 2161–2169, 1996. (Cited on page 16.)

[26] CRTonline: Fda approves edwards's sapien heart valve trial. 2008.
Available at: `http://www.crtonline.org/pr.aspx?PAGE_ID=4057` (Cited on page 19.)

[27] Iso 5840 international standard for cardiac valve prostheses. 2005. (Cited on pages 21 and 22.)

[28] Chikwe, J., Walther, A. and Pepper, J.: The surgical management of aortic valve disease. *British Journal of Cardiology*, vol. 6, pp. 453–461, 2003. (Cited on page 25.)

[29] Lifeciences, E.: Edwards sapien transcatheter heart valve.
Available at: `http://www.edwards.com/products/percutaneousvalves/sapienthv.htm` (Cited on pages 30 and 95.)

[30] *Marc 2007 r1 - Volume B: Element Library*, . (Cited on page 35.)

[31] Visser, G.: E-mail correspondecse with author, 1 november 2007. (Cited on page 37.)

[32] Xia, Z., Ju, F. and Sasaki, K.: A general finite element analysis method for balloon expandable stents based on repeated unit cell (ruc) model. *Finite Elements in Analysis and Design*, vol. 43, pp. 649–658, 2007. (Cited on page 38.)

[33] Stuparu, M.: Human heart valves, hyperelastic material modeling. Tech. Rep., University of Timisoara, 2002. (Cited on page 38.)

[34] Mark, A.: Applications of high pressure balloons in the medical device industry. Tech. Rep., Advanced Polymers Inc., 1999. (Cited on page 38.)

[35] J.E. Shigley, C.R.M. and Budynas, R.: *Mechanical Engineering Design: Seventh Edition*. McGraw-Hill Higher Education, 2003. (Cited on pages 51 and 56.)

[36] Marrey, Ramesh V, e.a.: Fatigue and life prediction for cobalt-chromium stents: A fracture mechanics analysis. *Biomaterials*, vol. 27, pp. 1988–2000, 2006. (Cited on pages 51 and 55.)

[37] Stainless, A.: Grades of stainless steel - grade 316. 2007.
Available at: `http://www.fanagalo.co.za/tech/tech_grade_316.htm` (Cited on page 55.)

[38] D. Aslanidis, G. Roebben, J.B. and van Moorleghem, W.: Electropolishing for medical devices: Relatively new... fascinatingly diverse. Tech. Rep., @medical technologies n.v. (AMT), 2001. (Cited on page 65.)

[39] Lehmann, M.: E-mail correspondence with author, 5 june 2008.: Stainless steel 316l stents - electropolishing procedure and electropolish composition. (Cited on page 65.)

[40] Dumoulin, C. and Cochelin, B.: Mechanical behaviour modelling of balloon-expandable stents. *Journal of Biomechanics*, vol. 33, pp. 1461–1470, 2000. (Cited on pages 74 and 94.)

[41] Johnson & johnson gateway.
Available at: `http://www.jnjgateway.com` (Cited on page 94.)

[42] David Chua, S., MacDonald, B. and Hashmi, M.: Finite-element simulation of stent expansion. *Journal of Materials Processing Technology*, vol. 120, pp. 335–340, 2002. (Cited on page 94.)

[43] Migliavacca, F.e.a.: Mechanical behavior of coronary stents investigated through the finite element method. *Journal of Biomechanics*, vol. 35, pp. 803–811, 2002. (Cited on page 94.)

Appendices

Appendix A

Stent Design Concepts

A.1 Stent Concept: Design 1

The concept for Design 1 was based on the Palmaz-Schatz [40; 41; 42; 43] coronay stent from Johnson & Johnson Medical Devices. This design consists of a tube with simple square slots which appear like diamond shaped cells after expansion. Figure A.1 and Figure A.3 respectively shows the undeformed initial geometry and fully expanded configuration of the stent. Due to the cyclic radial symmetry of the stent, the initial expansion, crimping and rigid deployment process was simulated for only one seventh of the stent. The results of the simulation was then revolved to show the complete stent. From Figure A.3 it can be seen that the stent has 14 distal protrusion annexes. However the three leaflets of the valve assembly require three assembly joints, equi-spaced around the diameter of the stent. For this reason, an ideal stent for the assembly must have a number of distal protrusion annexes which is a multiple of three. The total equivalent plastic strain after the deployment process is in excess of 60% (see Figure A.3) and the strain-limit of Stainless Steel 316L is 43%. Figure A.2 shows the crimped state of the stent. From the figure, it can be seen that the stent experiences severe non-uniform deformation during the crimping process. Given the factors discussed in the previous paragraph, it is apparent that this stent design is not suitable for a

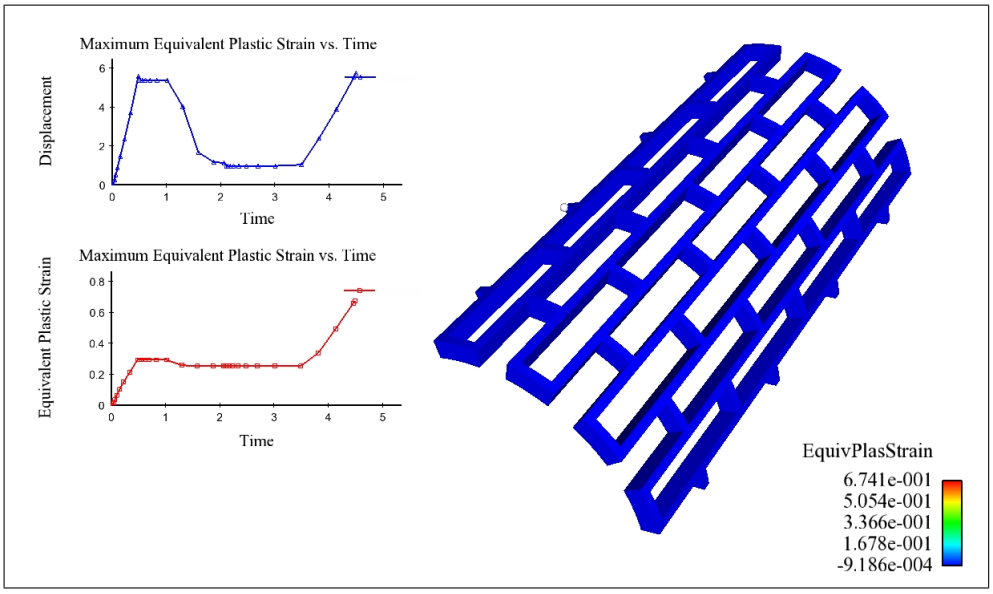

Figure A.1: Stent Design 1: Undeformed State

percutaneous aortic valve application, and the design was subsequently rejected as a feasible concept.

A.2 Stent Concept: Design 2

The concept for Design 2 was based on the stent used in the Edwards SAPIEN Transcatheter Heart Valve from Edwards Life Sciences [29]. This design consists of three support props, which serve as assembly joints for the three leaflets of the valve. The support props are connected with two sets of mirrored zig-zag shaped struts, which enable the crimping and expansion of the stent. Figure A.4 and Figure A.6 respectively shows the undeformed initial geometry and fully expanded configuration of the stent. Due to the cyclic radial symmetry of the stent, the initial expansion, crimping and rigid deployment process was simulated for only one third of the stent. The results of the simulation was then revolved to show the complete stent. It can be seen form Figure A.5, which indicates the crimped state of the stent, that the stent performs well under the crimping process. The design differs from the Edwards SAPIEN design

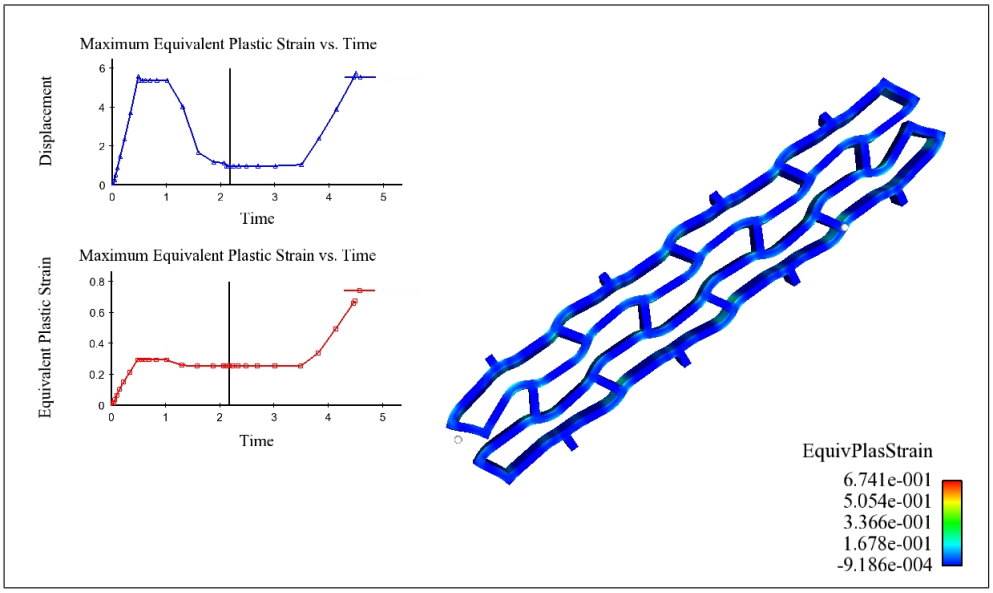

Figure A.2: Stent Design 1: Crimped State

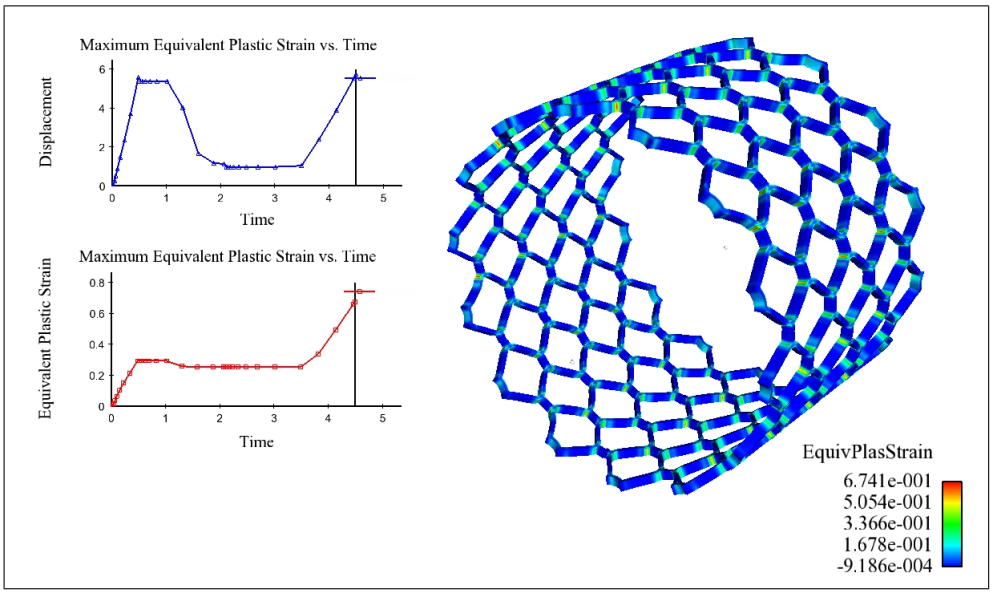

Figure A.3: Stent Design 1: Deployed State

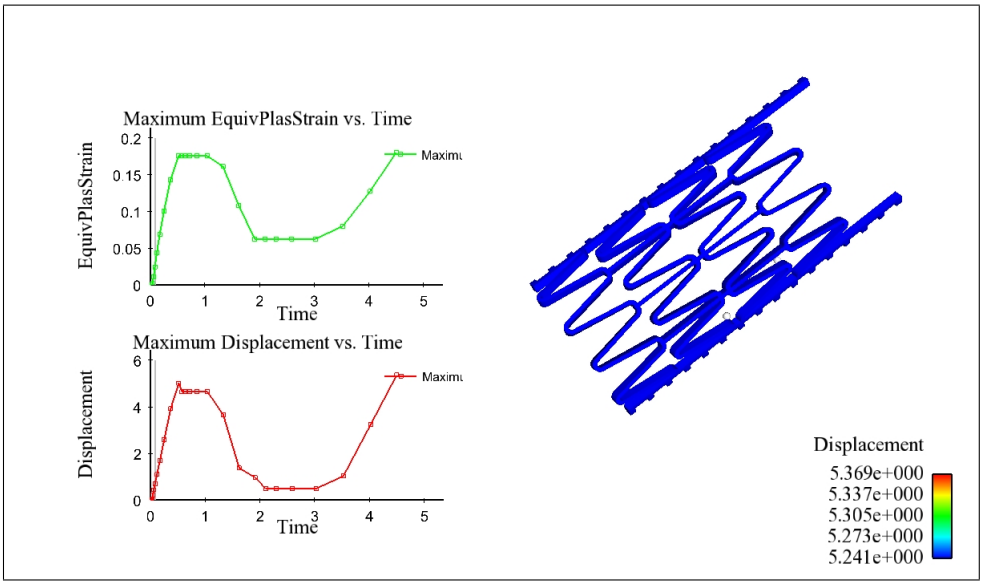

Figure A.4: Stent Design 2: Undeformed State

in that the support props extend well beyond the final row of stuts (See Figure A.4). This is to allow for a maximum stent length, while preventing coronary obstruction from the stent. Maximizing the stent length is advantageous as it allows for more room to seal the stent (which prevents regurgitation), given the minimum required stent length to assemble the valve leaflets. A simplified fatigue analysis was conducted of the predicted cyclic forces as experienced by the support props during the valve operation (Details of the fatigue analysis are given in section 5.8). Figure A.7 shows the maximum stress state of the fatigue analysis. The analysis indicated that the safety factor against fatigue was 1.15. Given that the required FSF was given as 1.5 (see section 3.1), this design did not conform to the engineering requirements and was subsequently rejected. None the less, the design served as the basis for further concept development.

A.3 Stent Concept: Design 3

The concept for Design 3 consists of a zig-zag strut pattern (along the stent circumference) which has been duplicated and translated along the

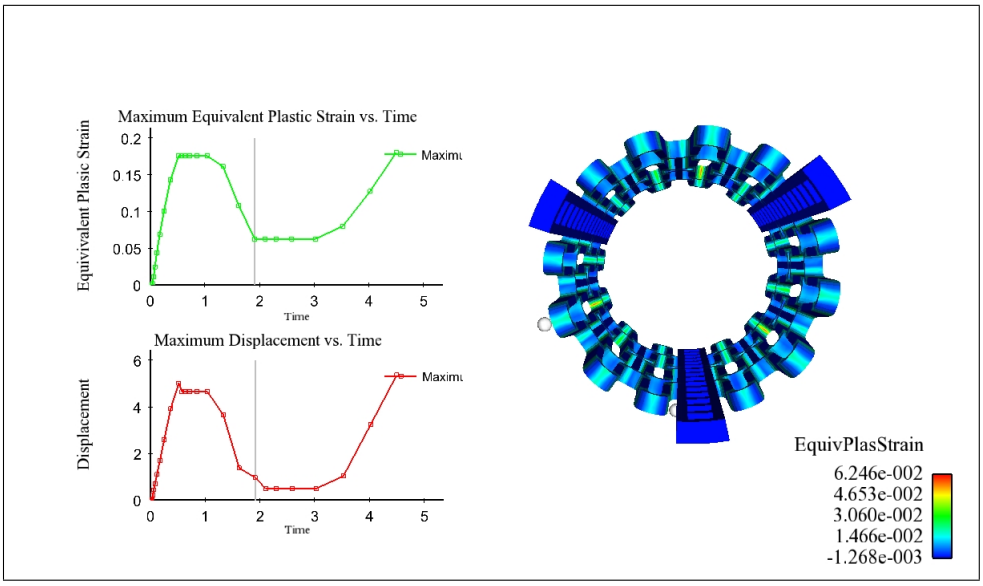

Figure A.5: Stent Design 2: Crimped State

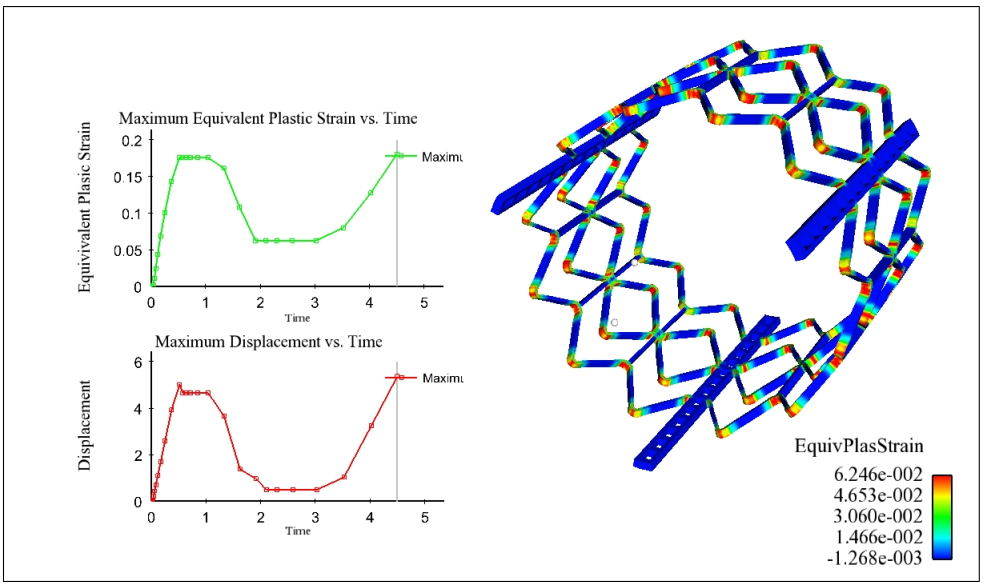

Figure A.6: Stent Design 2: Deployed State

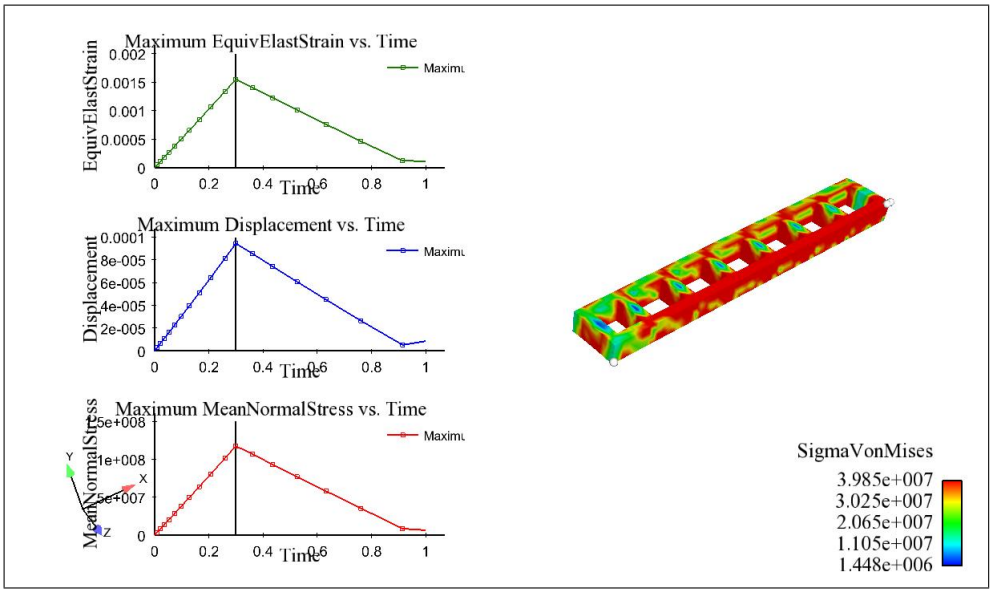

Figure A.7: Stent Design 2: Fatigue Analysis

axial direction. The zig-zag strut patterns are inter-connected with straight axial struts. The zig-zag strut pattern enables the crimping and expansion of the stent, while the straight struts provide the structural support for the stent. Figure A.8 and Figure A.10 respectively shows the undeformed initial geometry and fully expanded configuration of the stent. Due to the cyclic radial symmetry of the stent, the initial expansion, crimping and rigid deployment process was simulated for only one twelth of the stent. The results of the simulation was then revolved to show the complete stent. It can be seen form Figure A.9, which indicates the crimped state of the stent, that the stent performs well under the crimping process. The concept was more suitable for the *parabolic* leaflets as compared to the *straight* leaflets. However, the strut alignment at the deployed state was not ideal for a parabolic leaflet assembly. Given the stent-leaflet slight incompatibility, the stent concept was rejected.

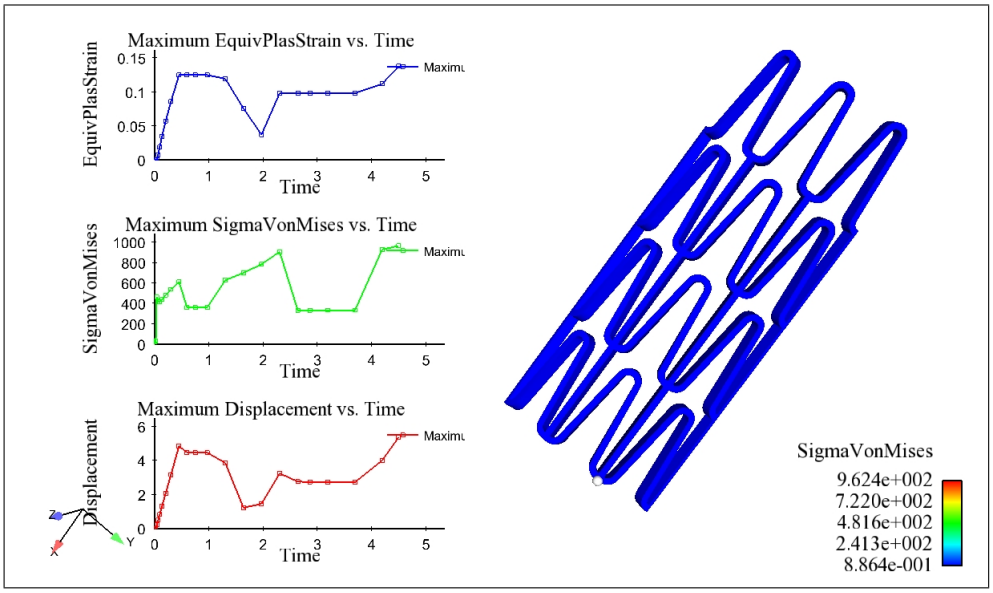

Figure A.8: Stent Design 3: Undeformed State

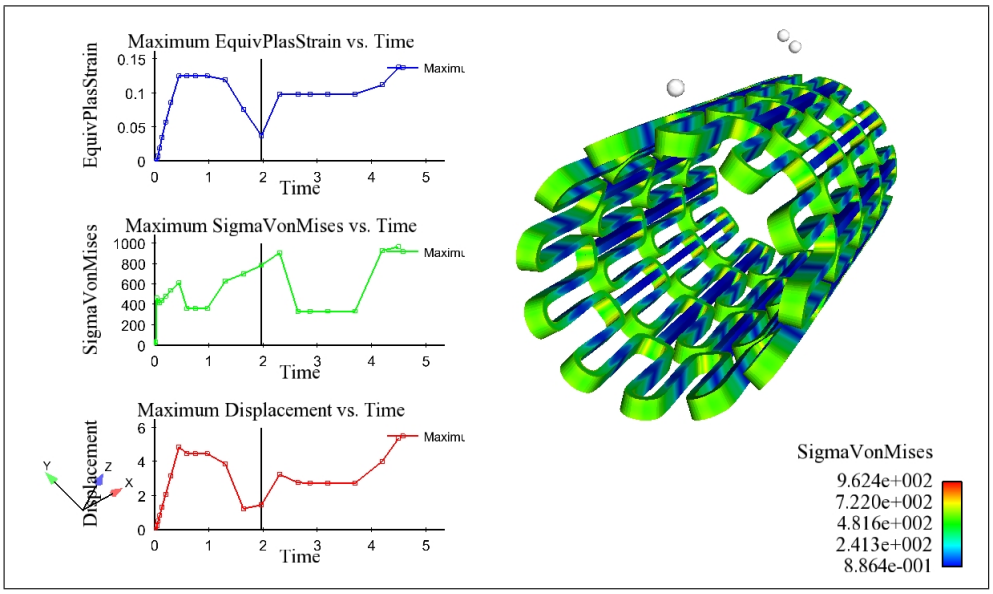

Figure A.9: Stent Design 3: Crimped State

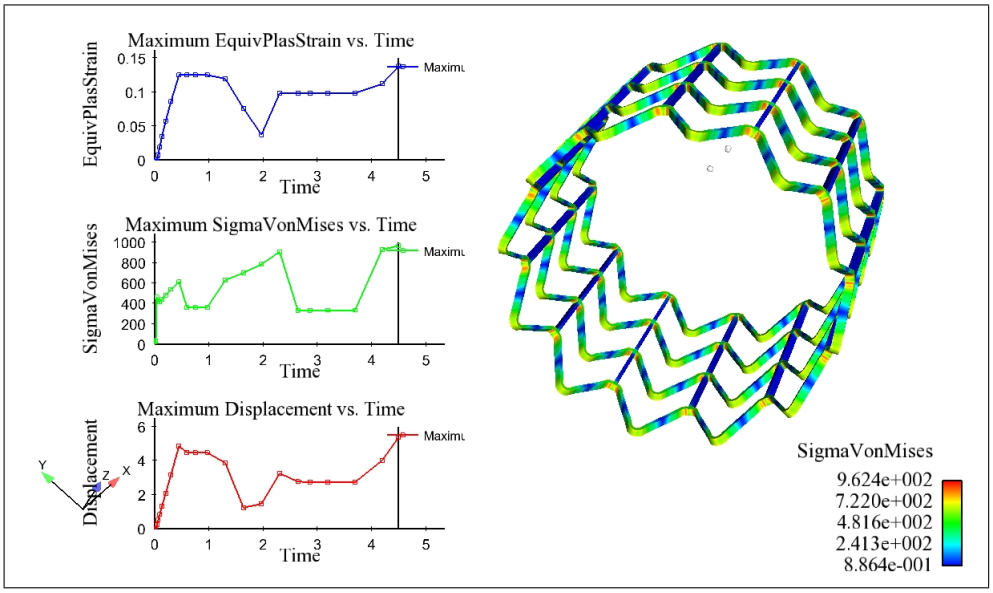

Figure A.10: Stent Design 3: Deployed State

Appendix B

FEM Boundary Conditions

B.1 Concept A

The red element faces in Figure B.1 indicate the planes of cyclic symmetry for Concept A. The nodes in the planes of cyclic symmetry were constrained to only allow for axial and radial translation in the symmetry planes. The orange marker indicates the node that was subjected to axial constraints to prevent the rigid body translation of the model.

B.2 Concept B

The red element faces in Figure B.2 indicate the planes of cyclic symmetry for Concept B. The nodes in the planes of cyclic symmetry were constrained to only allow for axial and radial translation in the symmetry planes. The orange marker indicates the node that was subjected to axial constraints to prevent the rigid body translation of the model.

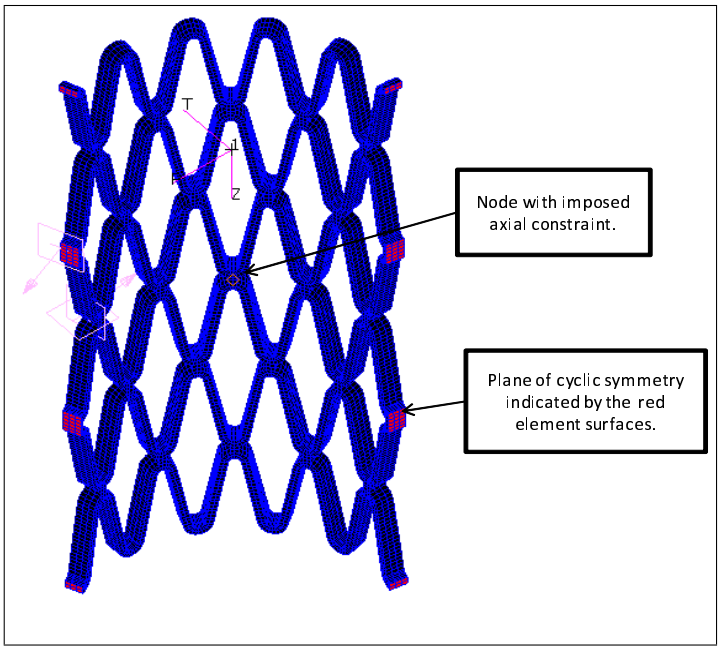

Figure B.1: Concept A: Displacement Constraints

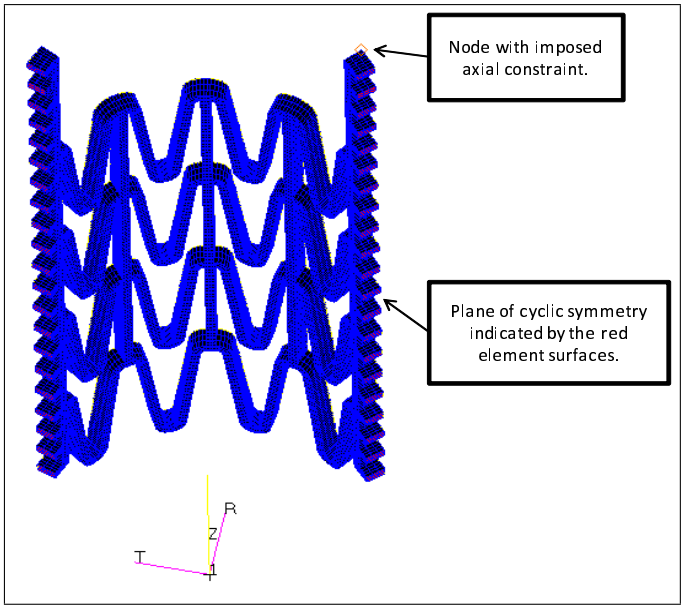

Figure B.2: Concept B: Displacement Constraints

Appendix C

Concept B - Load Steps

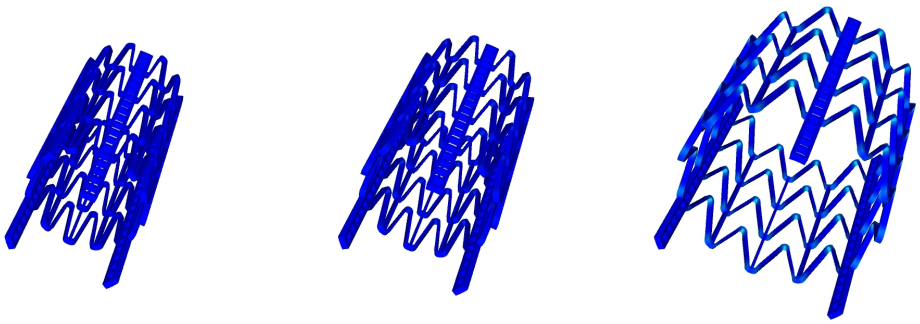

Figure C.1: Assembly Expansion Load Step

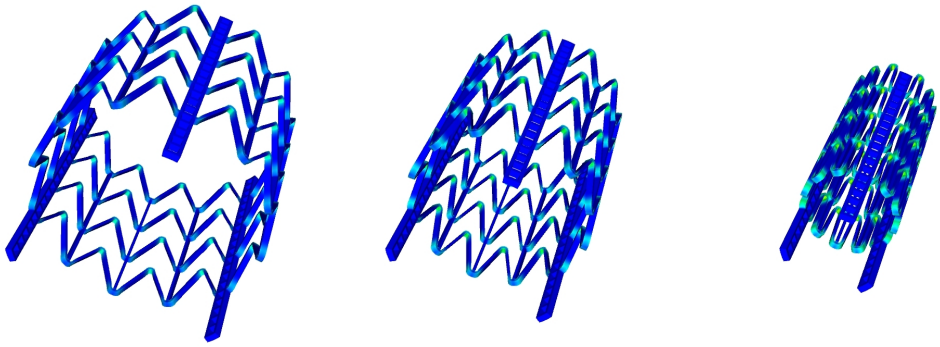

Figure C.2: Crimping Load Step

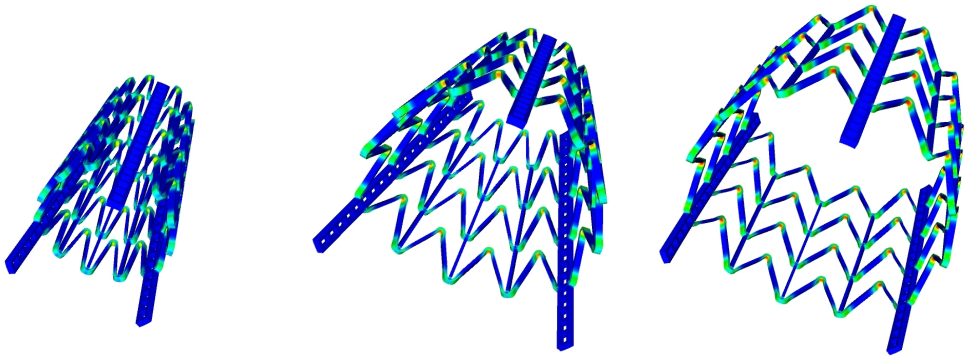

Figure C.3: Deployment Load Step

Appendix D

Electropolished Samples

Figure D.1 shows a magnified image of an untreated tubing sample. Figures D.2 to D.9 shows magnified images of tubing samples that were electropolished, each with different parameters. The parameters that were used for each sample is given in table D.1.

Figure D.1: Untreated Sample

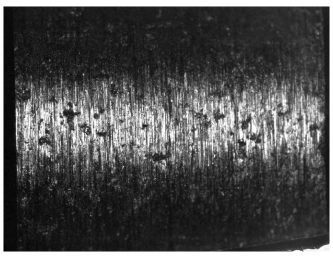

Figure D.2: Sample 1

Figure D.3: Sample 2

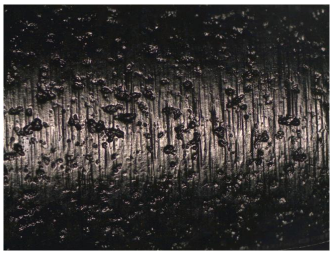

Figure D.4: Sample 3

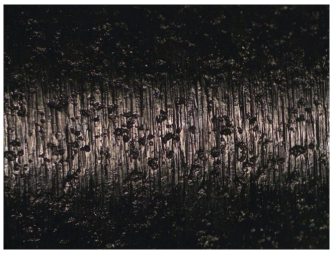

Figure D.5: Sample 4

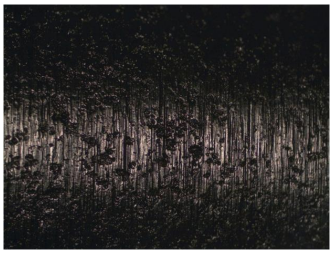

Figure D.6: Sample 5

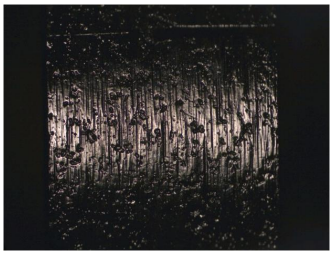

Figure D.7: Sample 6

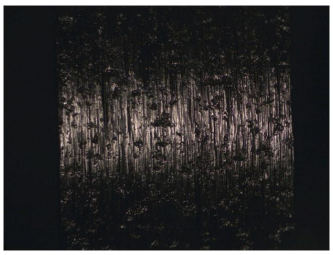

Figure D.8: Sample 7

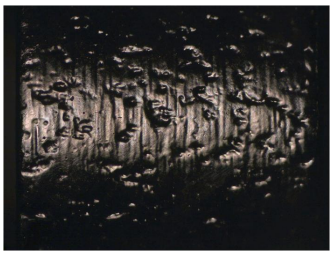

Figure D.9: Sample 8

Table D.1: Electropolished Sample Tubing: Parameters

	Voltage (V)	Agitation	Temperature (Degrees)	Processing Time (s)
Sample 1	16	3/6	72	90
Sample 2	16	3/6	70	120
Sample 3	16	3/6	70	135
Sample 4	16	3/6	80	75
Sample 5	16	3/6	72	150
Sample 6	16	3/6	73	120
Sample 7	16	3/6	72	105
Sample 8	16	3/6	88	135

Appendix E

Fatigue Analysis: MATLAB Code

```
clear all
close all

%Load MSC.Marc Report File
load CoreValve_fatigue_020.rpt;

%Write File to Variable
data = CoreValve_fatigue_020(:,3);

%Declare Variables

    %Number of Timesteps
Timesteps = 19;

    %Number of Elements
Elements = length(data)/19;

    %Fatigue Limit
sigma_e = 260;

    %True Ultimate Tensile Strength
```

```
sigma_ut = 965;

%Organise Data into Columns
for ii = 0:Elements - 1
for jj = 1:Timesteps
data1(jj,ii+1) = data(ii*9+jj);
end
end

%Get max and min principle stresses for each element
for ii = 1:Elements
max_prin_stress(ii) = max(data1(:,ii));
min_prin_stress(ii) = min(data1(:,ii));
end

%Calculate mean stress ans stress ampliture for each element
for ii = 1:Elements
stress_mean(ii) = (max_prin_stress(ii)+min_prin_stress(ii))/2;
stress_amp(ii) = abs((max_prin_stress(ii)-min_prin_stress(ii))/2);
end

%Ignore Elements in Compression
jj = 1;
for ii = 1:Elements
if stress_mean(ii) >= 0
stress_mean1(jj) = stress_mean(ii);
stress_amp1(jj) = stress_amp(ii);
jj = jj + 1;
end
end

%Calculate Modified Goodman line
m = -sigma_e/sigma_ut;
```

```
x = 0:sigma_ut;
y = m*x + sigma_e;

%Calculate Data Point Nearest to Goodman Line
for ii = 1:length(stress_mean1)
c = stress_amp1(ii) - (-m)*stress_mean1(ii);
x1 = (c-260)/(2*m);
y1 = -m*x1+c;
dist(ii) = sqrt(((stress_amp1(ii)-y1)^2+(stress_mean1(ii)-x1)^2));
end

    %Calculate min distance
min_dist = min(dist);

    %Position of worst case data point
position = find(dist == min_dist);
    %Worst Case Mean Stress
wc_stress_mean = stress_mean1(position)

    %Worst Case Stress Amplitude
wc_stress_amp = stress_amp1(position)

%Get Worst Case Element Number
wc_Element = find(stress_mean == wc_stress_mean)

%Calculate Safety Factor Against Fatigue
SF = 1/((wc_stress_amp)/(260)+(wc_stress_mean)/(965))

%Plot Data and Write Figure to 'eps' file
plot(stress_mean1,stress_amp1,'.','markersize',4); %Plot Data
hold on
plot(x,y,'r','linewidth',2);
grid on
```

```
xlabel('Predicted Mean Stress (MPa)');
ylabel('Predicted Stress Amplitude (MPa)');
legend('FEM Data','Modified Goodman Line');
plot(wc_stress_mean,wc_stress_amp,'x','markersize',6);
print('-depsc','-r600','CoreValve020.eps')
```

Appendix F

Fatigue Analysis: Results

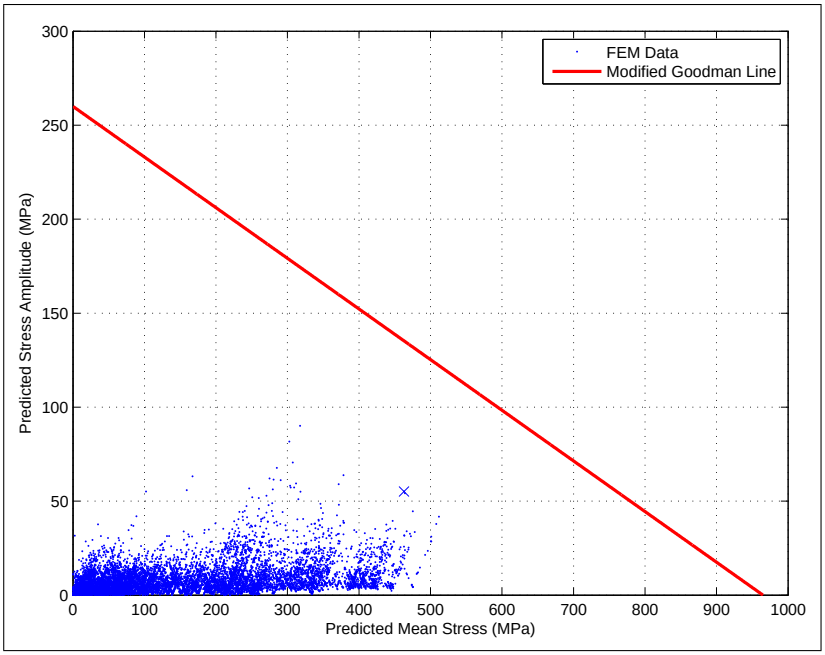

Figure F.1: Concept A: Fatigue Diagram - Strut Width 0.20 mm

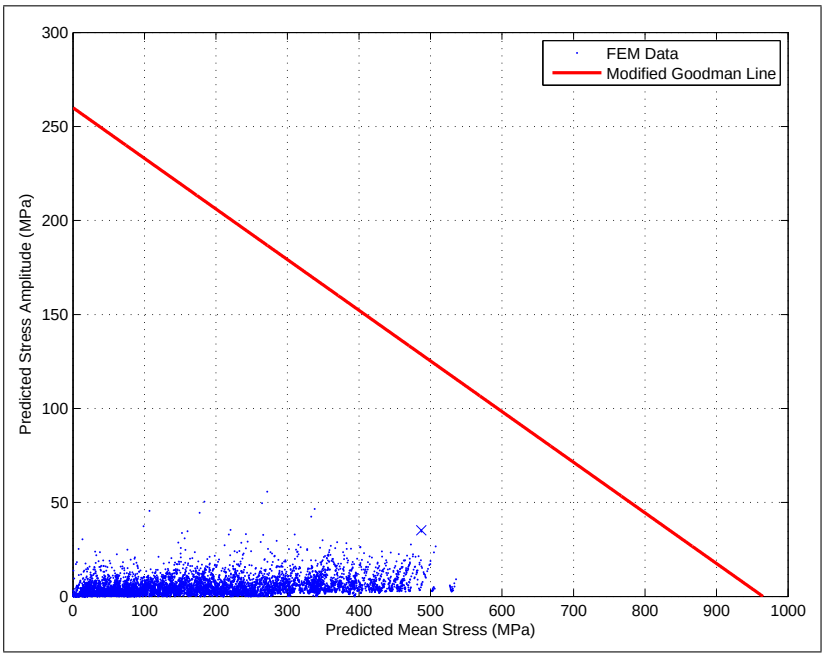

Figure F.2: Concept A: Fatigue Diagram - Strut Width 0.25 mm

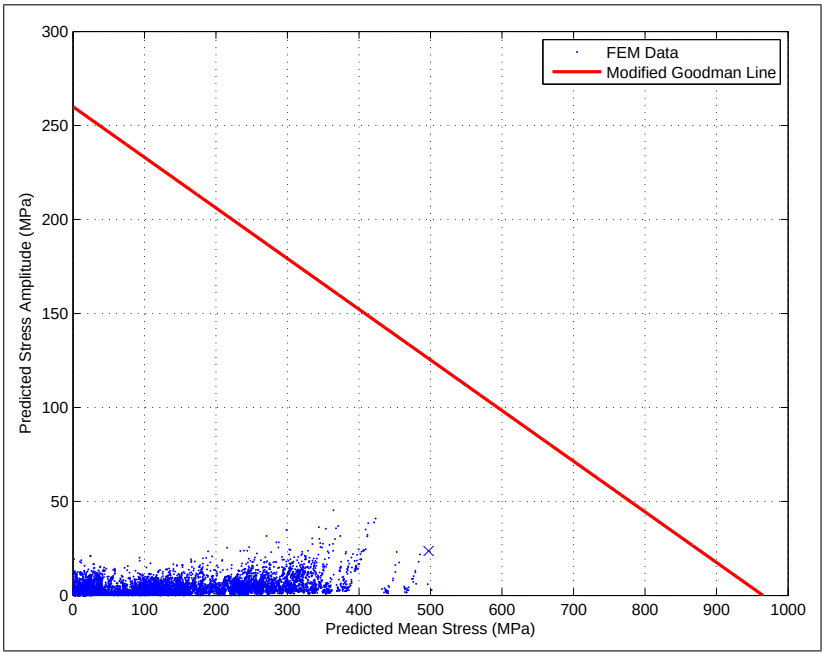

Figure F.3: Concept A: Fatigue Diagram - Strut Width 0.27 mm

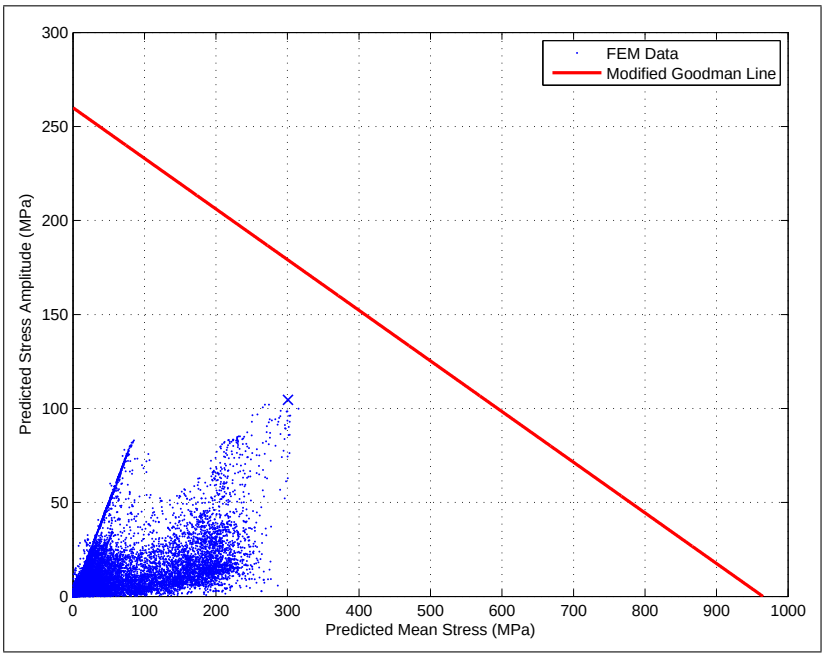

Figure F.4: Concept B: Fatigue Diagram - Strut Width 0.20 mm

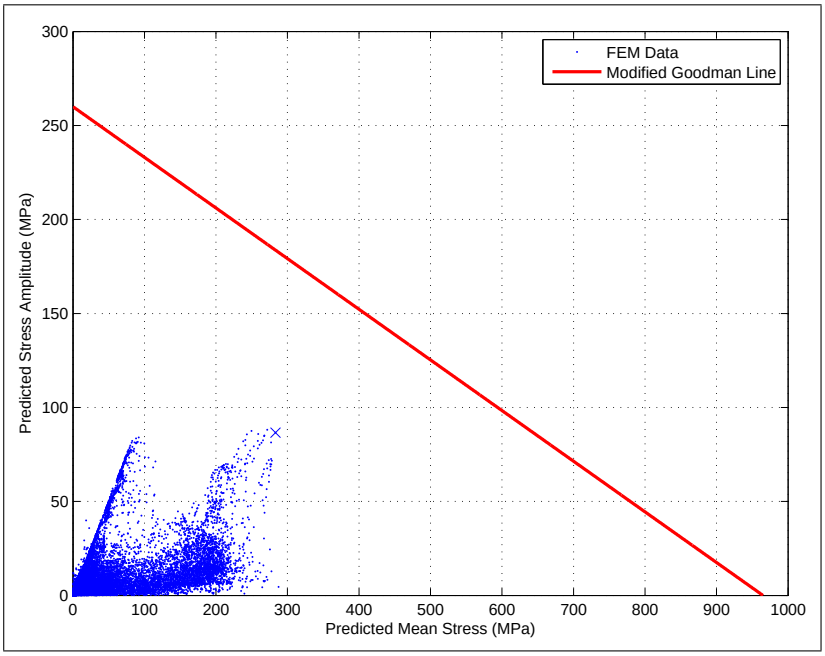

Figure F.5: Concept B: Fatigue Diagram - Strut Width 0.22 mm

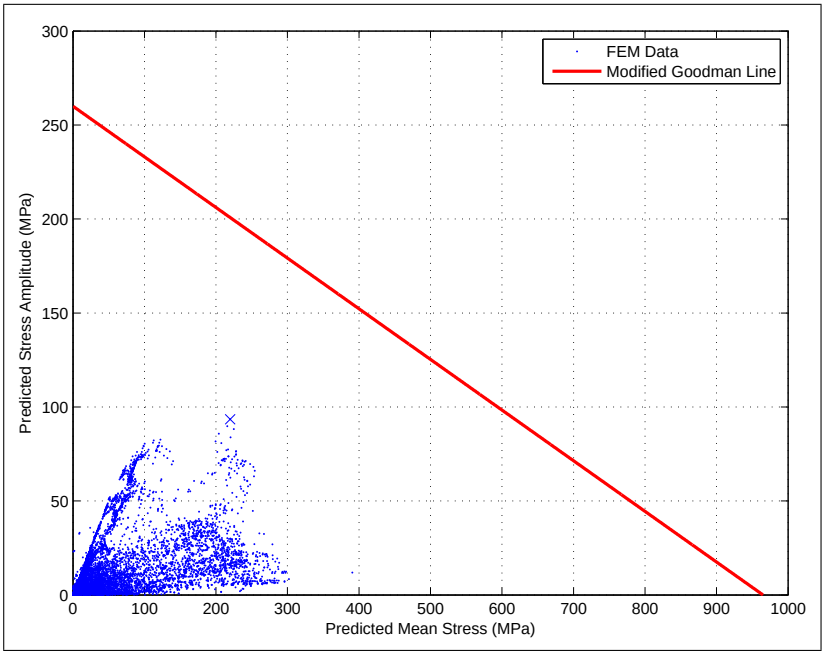

Figure F.6: Concept B: Fatigue Diagram - Strut Width 0.27 mm

Appendix G

Concept A: Second Iteration

Figure G.1 shows the suggested dimensions for the second iteration of Concept A.

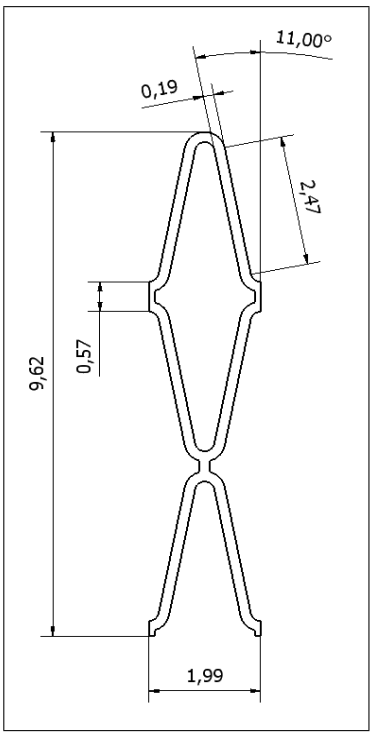

Figure G.1: Concept A: Second Iteration